uOttawa

L'Université canadienne
Canada's university

FACULTÉ DES ÉTUDES SUPÉRIEURES ET POSTDOCTORALES

uOttawa

L'Université canadienne
Canada's university

FACULTY OF GRADUATE AND POSTDOCTORAL STUDIES

Richard Daviau
AUTEUR DE LA THÈSE / AUTHOR OF THESIS

M.Sc. (Electrical Engineering)
GRADE / DEGREE

Department of Electrical Engineering
FACULTÉ, ÉCOLE, DÉPARTEMENT / FACULTY, SCHOOL, DEPARTMENT

Fabrication of Surface Plasmon Waveguides on Cytop

TITRE DE LA THÈSE / TITLE OF THESIS

P. Berini
DIRECTEUR (DIRECTRICE) DE LA THÈSE / THESIS SUPERVISOR

N. R. Tait
CO-DIRECTEUR (CO-DIRECTRICE) DE LA THÈSE / THESIS CO-SUPERVISOR

EXAMINATEURS (EXAMINATRICES) DE LA THÈSE / THESIS EXAMINERS

H. Anis

G. Tarr

Gary W. Slater
Le Doyen de la Faculté des études supérieures et postdoctorales / Dean of the Faculty of Graduate and Postdoctoral Studies

Fabrication of surface plasmon waveguides on Cytop

by
Richard Daviau

A Thesis submitted to the Faculty of Graduate Studies and Post-doctoral Studies in partial fulfillment of the requirements for the degree of Master of Applied Science in Electrical Engineering

05/05/2009

Ottawa-Carleton Institute for Electrical and Computer Engineering
School of Information Technology and Engineering
University of Ottawa
Ottawa, Ontario, Canada

Your file Votre référence
ISBN: 978-0-494-58193-3
Our file Notre référence
ISBN: 978-0-494-58193-3

Table of Contents

Abstract

This thesis discusses Surface Plasmon waveguides on Cytop and is divided into two topics. The first topic covers the fabrication and physical characterization of thin metal stripe waveguides on Cytop. The fabrication process is fully described and generally consists of a Cytop layer deposition and cure process and a bi-layer metal liftoff process. Physical characterisation was conducted on structures having undergone intermediate process steps and on finished structures, and results are presented and discussed. Optical microsope, SEM, AFM inspections and Metricon measurements were used to characterize the devices. Working waveguides on finished device wafers were confirmed by observing infrared images of output modes.

The second topic describes and presents the attenuation measurements and the technique used for exciting the surface plasmons of the fabricated waveguides. The technique uses a tapered polarization maintaining optical fibre positioned in direct contact with the structure such that the slow mode of the fibre couples through partial modal overlap to the surface Plasmon propagating thereon.

Acknowledgements

I dedicate this work to all those who have helped me through a difficult two and a half years. There were many moments where I was about to throw in the towel and not look back, but those close to me supported me through the worst of times.

I would like to thank Mom for being strong and supportive and reminding me that I got my genes from her. A quick thanks to Bob, Jamie, Christine, Cindy, Rob, Alex, John and Sunita.

I would like to thank Dr. Pierre Berini for giving me the opportunity to do my Masters degree (even though I was three years out of university) and for his guidance and being patient with me as this writing process took (much) longer than expected. I would also like to thank Dr. Niall Tait for being my co-supervisor and helping me out in the fabrication lab.

Special thanks to Norman Fong for being a great fabrication lab partner. I would also like to thank Ewa, Robin, Israel, Charles, Michael and Federico for all your input and help.

Chapter 1

Introduction

Writing of thesis and papers

- The first, second and final drafts of the thesis paper were written by me. The thesis was revised by Dr. Berini and Dr. Tait.

1.1 - Single Interface Surface Plasmons and (Bio)chemical sensing

Transverse Magnetic (TM) optical surface waves that propagate along the interface between a metal and dielectric are called Surface Plasmon-Polaritons (SPPs)[1]. This phenomenon is best explained by the knowledge that metals have a negative real part of permittivity at optical frequencies[2] and that TM surface waves are known to propagate along the interface between two materials that have a real part of the permittivity of opposite sign. The metal/dielectric interface is able to support an SPP mode at optical wavelengths which is confined by the coupling of electromagnetic waves to electron oscillations at the surface of the metal[3].

The derivation of the field solutions for the single interface SPP is given in Appendix A. From the derivation in Appendix A and Figure 1-1, we see that the fields are localized at the metal/dielectric interface and decay exponentially there from. This field localization property makes the SPP waveguides an ideal candidate for use in (bio)chemical sensing applications as it can be shown that a small change in the permittivity of the dielectric will greatly affect the propagation of the SPP. This subject matter has been covered by a number of published reviews written by Barnes[1,4] and Maier[5], for example.

---

[1] W. L. Barnes, J. Opt. A, Pure and Appl. Opt. 8 (2006) S87
[2] E. Palik, Handbook of Optical Constants of Solids. New York: Academic Press, 1985.
[3] A. D. Boardman, Electromagnetic Surface Modes. New York: Wiley, 1982.
[4] W. L. Barnes, A. Dereux, and T. W. Ebbesen, Nature, vol. 424, no. 6950, pp. 824–830, 2003.
[5] S. A. Maier and H. A. Atwater, Journal of Applied Physics, vol. 98, no. 1, p. 10, 2005.

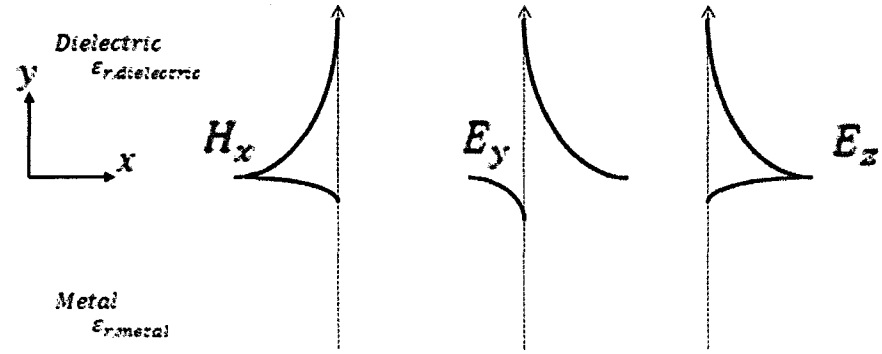

Figure 1-1: Diagram representing the metal/dielectric interface as well as field components of the SPP mode. Relative signs of the field components are properly represented, positive (+) to the right of the dotted line and negative (-) to the left. Relative magnitudes are not preserved.

Bio(chemical) sensing is usually conducted using aqueous (buffer) solutions which contain mostly water and so when using a long-range surface Plasmon-polariton (LRSPP) device for (bio)chemical sensing it is desirable to use low-index dielectrics which closely match the index of water[6] so that the index difference is minimized. The LRSPP wave will be discussed in greater detail in Section 1.3. Two such dielectric materials which have indexes close to water are Cytop and Teflon; a number of (bio)chemical sensing devices using SPPs and these two materials have been fabricated[7,8,9]. The advantage of using these materials in an LRSPP configuration is that they can be made as an integrated chip using well known fabrication techniques as well as an improved surface sensitivity and detection limit.

This thesis discusses the fabrication and testing of thin Au stripe waveguides on Cytop operating in the ss_b^0 (LRSPP) mode. The next two sections will provide a brief description of the thin film metal stripe waveguide; which is followed by a section discussing the motivation and an implementation of its use as a (bio)chemical sensing device. The point of novelty is that this is the first time that Cytop has been used to fabricate LRSPP waveguides.

---

[6] D. J. Segelstein, M.Sc. Thesis, University of Missouri, Kansas City, 1981.
[7] J. Dostálek, A. Kasry, and W. Knoll, Plasmonics 2 (2007) 97.
[8] A. W. Wark, H. J. Lee, R. M. Com, Analytical Chemistry 77 (2005) 3904.
[9] A. Kasry and W. Knoll, App. Phys. Lett. 89 (2006) 101106.

1.2 - Thin Metal Slab sandwiched by a dielectric

If the metal is made into a thin film then the SPP modes of the top and bottom interface are able to couple to one another to form super-modes[5] offering 1-dimensional field confinement. Using a method similar to the derivation shown in Appendix A it can be shown that for a dielectric/metal/dielectric combination, as depicted in Figure 1-2, that the metal film can support a symmetrical coupled bound (s_b) mode. The s_b mode exhibits dispersion with film thickness[10]. As the metal film thickness is reduced the propagation constant of the s_b mode tends toward that of a transverse magnetic (TEM) wave propagating in a medium having the permittivity of the dielectric regions[10]. As the metal film increases in thickness the super-mode uncouples and the propagation constant of the s_b mode tend towards that of a single interface SPP supported by the metal/dielectric interface[10].

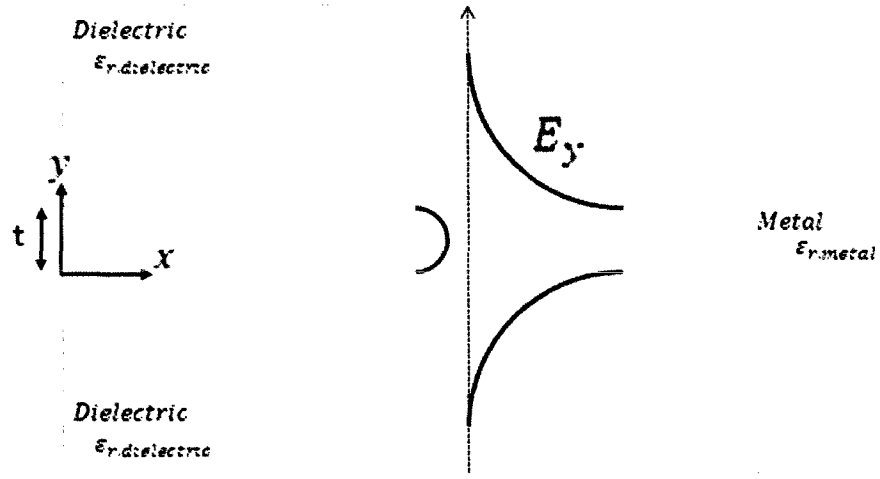

Figure 1-2: Diagram representing the dielectric/metal/dielectric configuration as well as the main transverse field component of the symmetrical coupled bound (s_b) mode. Relative signs of the field components are properly represented, positive (+) to the right of the dotted line and negative (-) to the left.

[10] P. Berini, Physical Review B, 61 (2000) 10484

1.3 - Thin Film Metal Stripe surrounded by a dielectric background

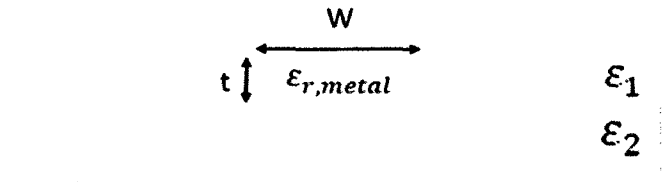

Figure 1-3: Cross-sectional view of the thin metal stripe waveguide

If the metal is made into a thin metal film of finite width and surrounded by dielectric, as shown in Figure 1-3, the metal stripe provides 2-dimensional field confinement allowing it to be used as a waveguide. The waveguide supports (when $\varepsilon_1 = \varepsilon_2$) as a fundamental mode, a long-range (low-loss) surface Plasmon-polariton wave denoted as the ss_b^0 mode[10]. A number of passive optical elements such as S-bends, Y-junctions, Couplers, Mach-Zehnders[11,12,13] have been fabricated using the thin metal stripe and operated in the LRSPP. A metal stripe on a substrate exposed to air[14] ($\varepsilon_{r,1}$=1) can also support SPPs but these are generally not the not the long-range SPP found in a highly symmetric structure ($\varepsilon_1 = \varepsilon_2$)[10]. The metal stripe waveguide of Figure 1-3 is the basic structure that this thesis is concerned with.

Figure 1-4 shows the evolution of the spatial distribution of Re{E_y} of the LRSPP over the waveguide cross section in Figure 1-3 as the index asymmetry increases; the upper cladding is the higher index medium. Figure 1-4 is adapted from reference[15], it is not an exact representation of the device fabricated in this thesis as reference[15] discusses the asymmetry of a metal stripe cladded in silica and in context of this thesis it is meant to give a representation of what is happening to the mode field. As the index asymmetry increases the ss_b^0 mode becomes leaky, radiating into the higher-index cladding as it

---

[11] R. Charbonneau, N. Lahoud, G. Mattiussi, and P. Berini, Opt. Express 13 (2005) 977.
[12] A. Boltasseva, T. Nikolajsen, K. Leosson, K. Kjaer, M. S. Larsen, and S. I. Bozhevolnyi, J. Light. Technol. 23 (2005) 413.
[13] R. Charbonneau, C. Scales, I. Breukelaar, S. Fafard, N. Lahoud, G. Mattiussi, and P. Berini, J. Light. Technol. 24 (2006) 477.
[14] J.C. Weeber, A. Dereux, C. Girard, J. R. Krenn, and J.P. Goudonnet, Phys. Rev. B 60 (1999) 9061.
[15] P. Berini, J. App. Phys., 102 (2007) 053105

propagates. For the devices discussed in this thesis, an index mismatch tolerance between the upper and lower claddings of 10^{-3} is required for the ss_b^0 to remain bounded to the metal stripe.

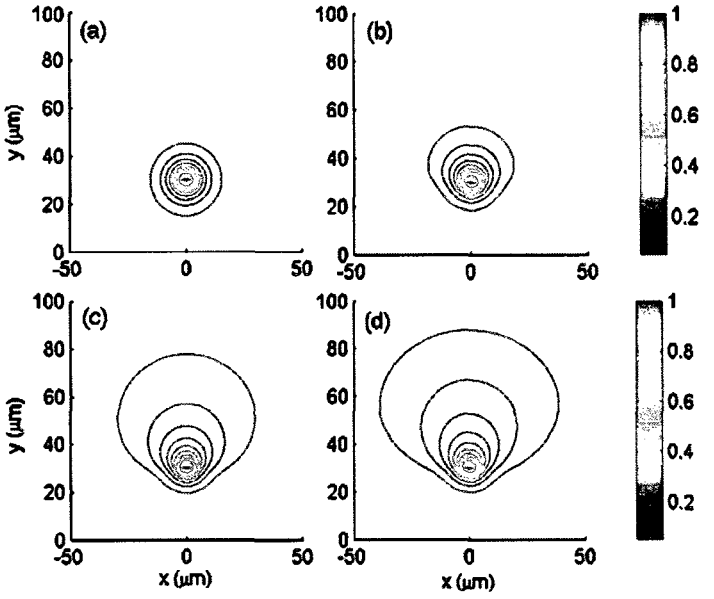

Figure 1-4: Representative diagram of the evolution of the spatial distribution of $Re\{E_y\}$ as the index asymmetry increases from ($\varepsilon_1 = \varepsilon_2$) to a large asymmetry ($\varepsilon_1 \neq \varepsilon_2$). The field is normalized such that max $|Re\{E_y\}|=1$. Adapted from Ref. 15.

1.4 - LRSPP Waveguide Architecture for use in (bio)chemical sensing

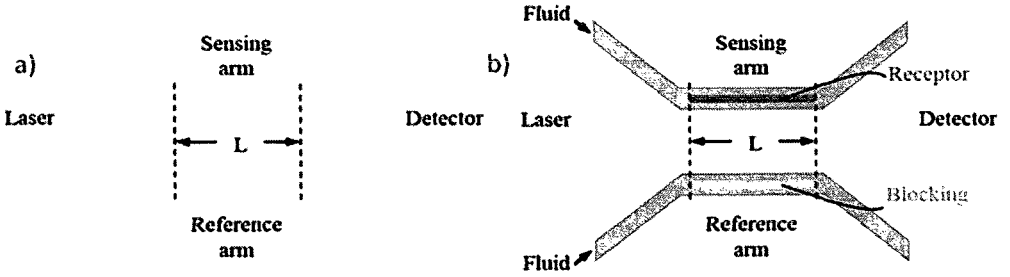

Figure 1-5: a) MZI using the metal stripe waveguide; b) MZI configured as an LRSPP (bio)chemical sensor. Adapted from Ref. 16.

One (bio)chemical sensor architecture that uses the metal stripe waveguide is the Mach-Zehnder interferometer (MZI) and is shown in Figure 1-5(a). Figure 1-5(b) shows the MZI configured as a (bio)chemical sensor; the upper cladding is fluidic and the flow of (bio)chemical fluids are controlled by inserting the chip in a flow cell. The LRSPP mode of the device is excited by butt-coupling the fibres through windows, the sensing arm is coated with receptor molecules targeted for a specific analyte and

the reference arm is coated with a blocking chemical. As the analyte in the carrier fluid flows over both arms and binds to the receptors the effective index of the sensing arm changes, which changes the optical path length of the sensing arm relative to the reference arm causing the output power of the MZI to vary. Figure 1-6 shows a cross-sectional view of the sensing arm of the MZI configured as a (bio)chemical sensor with an adlayer of thickness **a** containing the receptor molecules. The motivation for using this architecture as a (bio)chemical sensing device is that it has a high surface sensitivity to mode power attenuation ratio[16], allowing long optical interaction length sensors; the high surface sensitivity of this configuration has been demonstrated experimentally[17]. Currently, the Mach-Zehnder configuration used in (bio)chemical sensing devices have only been implemented using dielectric waveguides (e.g.: silicon on insulator (SOI)) technology. The advantage of implementing the Mach-Zehnder using the LRSPP is that there is a greater variety of surface chemistries that can be used on Au versus what can be used on a dielectric material.

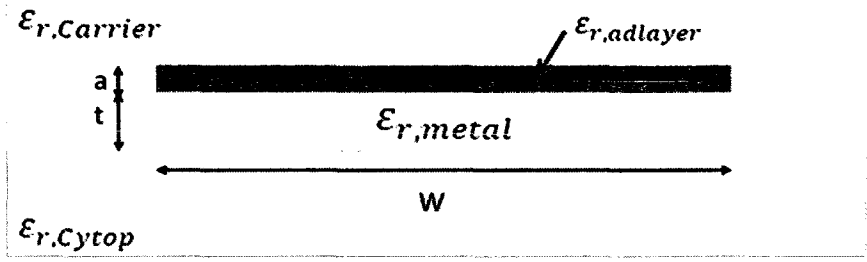

Figure 1-6: Cross-sectional view of the sensing arm of the MZI configured as a (bio)chemical sensor showing an adlayer containing the receptor molecule.

[16] P. Berini, New Journal of Physics, 10 (2008) 105010.
[17] R. Charbonneau, M. Tencer, N. Lahoud, P. Berini, Sensors and Actuators B: Chemical, 134 (2008) 455.

1.5 - Thesis Summary

This thesis consists of a collection of two submitted, but as of yet unpublished, articles.

Chapter 2 describes the fabrication and characterization of surface plasmon waveguides and integrated components on Cytop. The article discusses the full process flow from beginning to end and includes characterization results from Atomic Force Microscope and Metricon measurements. The article is incorporated into this thesis in a modified format different from the "as submitted" format.

Chapter 3 describes cut back measurements used to obtain the mode power attenuation of the surface Plasmon waveguides discussed in Chapter 2. The article also describes a novel technique of exciting the LRSPP mode using a tapered polarization maintaining fibre. The article is incorporated into this thesis in the "as published" format.

Chapter 4 contains concluding remarks and provides suggestions for future work using what has been developed through these studies.

Appendix A contains a derivation of the mode fields of a single interface surface Plasmon polariton.

Appendix B contains mode power attenuation measurements of Au stripes surrounded by silica.

Appendix C contains additional index of refraction and thickness measurements of Cytop.

Chapter 2

Fabrication of surface plasmon waveguides and integrated components on Cytop

Preamble

The paper discusses the fabrication and characterization of thin metal stripe waveguides and integrated components on Cytop. This is the first attempt at using Cytop as a low-index dielectric as a bottom cladding for thin metal stripe waveguides. The fabrication process flow and certain process steps are described. Physical characterisation was conducted on structures having undergone intermediate process steps and on finished structures, and results are given and discussed.

Contributions

The author gratefully acknowledges Robin Buckley (University of Ottawa) for conducting the simulations, Ewa Lisicka-Skrzek (University of Ottawa) for help with the optical experiments, Heng-Yong Nie of Surface Science Western for conducting the AFM measurements, and Norman Fong, Rob Vandusen and Carol Adams (Carleton University) for assistance with the fabrication.

Fabrication of surface plasmon waveguides and integrated components on Cytop

Richard Daviau

School of Information Technology and Engineering, University of Ottawa, 161 Louis Pasteur St., Ottawa, Ontario, Canada K1N 6N5, rdavi021@uottawa.ca

R. Niall Tait

Department of Electronics, Carleton University, 1125 Colonel By Drive, Ottawa, Ontario, Canada K1S 5B6, niall_tait@carleton.ca

Pierre Berini[18]

School of Information Technology and Engineering, University of Ottawa, 161 Louis Pasteur Street, Ottawa, Ontario, Canada K1N 6N5, berini@site.uottawa.ca, Department of Physics, University of Ottawa, Spectalis Corp., P.O. Box 72029, Kanata North RPO, Ottawa, Ontario, Canada K2K 2P4

Abstract - The fabrication and physical characterization of waveguides and integrated components on Cytop are described. The waveguides consist of a thin narrow Au stripe, on an optically infinite layer of Cytop. The integrated components implemented with this waveguide consist of Y-junctions, Mach-Zehnder interferometers and couplers. The waveguides and components are dimensioned such that they propagate long-range surface plasmon-polariton waves when cladded with an index-matched fluid. The fabrication process flow and individual process steps are described in detail. Physical characterisation was conducted on structures having undergone intermediate process steps and on finished structures, and results are given and

[18] Corresponding author

discussed. Working waveguides were verified by observing an output with an infrared camera. The waveguides and components are useful for (bio)chemical sensing in aqueous solutions.

Keywords: Cytop, Waveguide, Plasmon, Fabrication

1. Introduction

Surface plasmon-polaritons (SPPs) are transverse magnetic (TM) polarized optical surface waves that propagate along the interface between a metal and a dielectric [1]. Numerous plasmonic structures consisting of metal stripes or wires, plane or corrugated metal films, holes in metal films, or metal particles have been studied over time, exhibiting interesting and varied behaviour [2, 3].

The metal stripe [4-6] is an interesting plasmonic waveguide given the richness and complexity of its mode spectrum and its potential for applications. In the symmetric case, i.e. when the stripe is bounded above and below by media of the same refractive index, the waveguide supports as a fundamental mode, a long-range (low-loss) surface plasmon-polariton (LRSPP) wave, denoted as the ss_b^0 mode [4]. This mode was explored experimentally [7, 8], and the measured attenuation was compared with theory [9]. A number of passive optical elements such as S-bends, Y-junctions, couplers and Mach-Zehnders [10-13] have been fabricated using the thin metal stripe and operated in the LRSPP. The asymmetric structure [5], such as a metal stripe on a substrate exposed to air [6], can also support SPPs but they are generally not long-range.

LRSPPs are known to have a reasonably high surface sensitivity and a low attenuation [14], and thus have potential for use in (bio)chemical sensing, as demonstrated by

experimentation with a metal film in a prism-coupling geometry [15-18], and metal stripes in an integrated Mach-Zehnder interferometer (on SiO_2 and covered with index-matching oil) [19]. It is necessary to maintain index symmetry near the stripe in order for the LRSPP to be supported [4, 5]. For (bio)chemical sensing, this can be achieved by supporting the metal stripe with a thin optically not-too-invasive dielectric membrane and allowing the sensing fluid to surround the stripe [20, 21]. Alternatively, a dielectric material having an index which closely matches that of the sensing fluid can be used as a thick lower cladding supporting the stripe, and the sensing fluid allowed to flow over the stripe; this is the configuration of interest in this paper.

The sensing fluid in (bio)chemical sensing applications is typically an aqueous solution such as buffered de-ionised water, having an index that is slightly higher but close to that of pure water [22]. There are few materials that have an index close to that of water: two are Teflon [23] and Cytop [24], and both have been used for LRSPP (bio)chemical sensors in prism-coupled geometries [15-18]. Cytop has also been used to implement optical dielectric waveguides and components [25, 26], micro-machined devices [27] and electronic devices [28].

In this article, we describe the fabrication of LRSPP waveguides and integrated structures consisting of a thin Au stripe on a thick Cytop lower cladding. The fabrication approach involves a multiple spin-coat curing process and bi-layer metal lift-off to form the Au features. A number of physical characterization results obtained on structures having undergone intermediate process steps and on finished structures are presented. An optical output verifying the operation of a waveguide is given; further optical measurements are reported in [29]. The article is organized as follows: Sec. 2 details the process flow, Sec. 3 shows intermediate process steps, Sec. 4 shows finished devices, and Sec. 5 gives a brief summary with concluding remarks.

2. Waveguide structure, materials and process flow

2.1 Waveguide structure

Fig. 1(a) shows in front cross-sectional view the waveguide structure of interest, consisting of a thin Au stripe of width w, thickness t and relative permittivity $\varepsilon_{r,Au}$, supported by a Cytop lower cladding of thickness d and permittivity ε_2 (refractive index η_2), on a Si substrate of permittivity ε_{Si}. The stripe is bounded above by an index-matched sensing fluid of permittivity ε_1 (refractive index η_1), envisaged to flow within a flow cell.

Optical mode computations were performed numerically using COMSOL, which is a commercially available software based on the finite element method, for the structure depicted in Fig. 1(a), using $\eta_1 = \eta_2 = 1.3348$ (nominally) [24] and $\varepsilon_{r,Au} = -86.08 - j8.322$ [30] at a free-space operating wavelength of $\lambda_0 = 1310$ nm. The Cytop layer must be sufficiently thick such that the LRSPP is not affected by the presence of the Si wafer – the computations revealed that the bottom cladding should be at least d = 8 μm thick in order for this to be the case. Good dimensions for the Au stripe are t = 20 to 35 nm and w ~ 5 μm. Fig. 1(b) shows computed contours of $\mathrm{Re}\{E_y\}$ of the LRSPP supported by a t = 35 nm thick w = 5 μm wide Au stripe on optically infinite Cytop. The field distribution remains essentially symmetric about the plane of the stripe, and the mode long-ranging, as long as the index of the liquid above the stripe remains close to the index of Cytop to within a tolerance of $|\eta_1 - \eta_2| < 0.001$ (approximately). The LRSPP mode power attenuation of this nominal design is 7.2 dB/mm. These dimensions are considered good because the LRSPP mode remains bound to the stripe with reasonably low attenuation. If the dimensions were to increase (i.e. a thicker or wider stripe) the LRSPP mode would be more strongly attenuated and conversely if the dimensions were to decrease the LRSPP mode could be too weakly bound.

2.2 Materials

Cytop is an amorphous perfluoro-polymer developed by Asahi Glass Co [24]. It was chosen as the lower cladding material because it has a low index of refraction (slightly above that of water) and it has excellent transparency. The grade of Cytop chosen was CTL-809M (low molecular weight, 9% Cytop concentration dissolved in CT-SOLV180 perfluoro liquid solvent), because it has good adhesion to Si and metals without the need for extra adhesion layers and it can be spin-coated.

Au was chosen as the metal for the stripe due to its ability to support surface plasmons, its chemically stable nature, and its suitability for (bio)chemical sensor applications [15-18]. An adhesion layer is usually required to promote adhesion of Au to dielectrics, but we have found that Au sticks very well to Cytop without an adhesion promoting layer of e.g. Ti or Cr; this is an advantage because such adhesion metals are strongly absorbing.

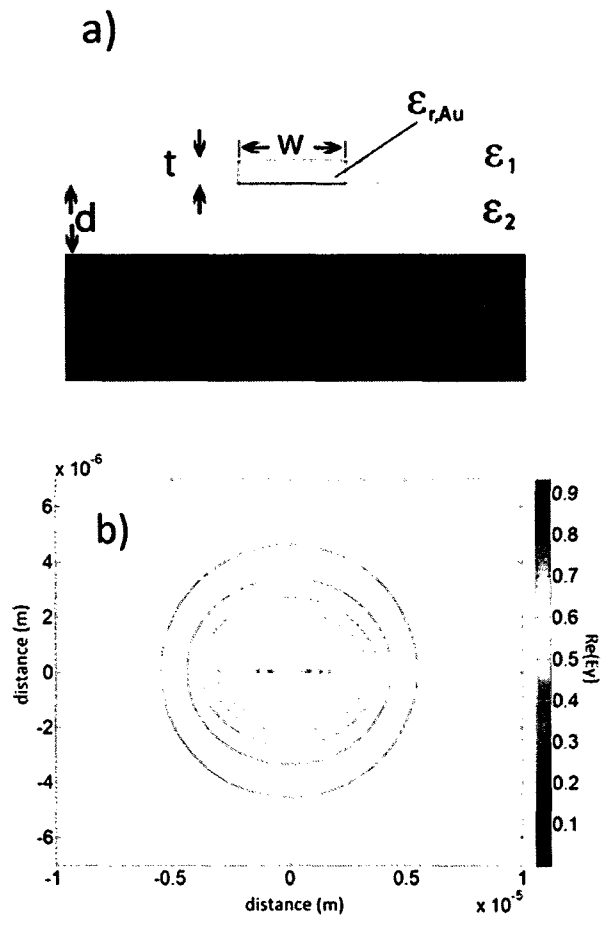

Figure 1: a) Cross-sectional view of the waveguide of interest and b) computed contours of Re{Ey} of the LRSPP mode supported by the structure.

2.3 Process flow

Table 1 describes the main process steps developed to fabricate the structure shown in Fig. 1 using these materials. The main process steps are depicted in Fig. 2.

The first step of the fabrication process is the cleaning and drying of the Si wafer that is to be used; we chose an O_2 microwave plasma etcher to dry the wafer, over the more conventional method of an oven bake, because it has been shown to improve the adhesion between the Si wafer and deposited polymer layers [31].

Step	Description	Fig. 2
1	Si wafer clean, HCl bath followed by O_2 plasma preen	a
2	Cytop layer deposition, multiple Cytop layer spin-coat/cure process	b
3	Cytop ashing, O_2 plasma etcher, 5 s, 100 W, 0.3 Torr O_2	
4	Lift-off photolithography, bi-layer re-entrant photoresist, contact mask aligner	c
5	Metal deposition, 35 nm Au, e-beam evaporation	d
6	Lithography removal, lift-off	e

Table 1: Main process steps for fabricating Au stripes on a thick Cytop lower cladding, with reference to Fig. 2

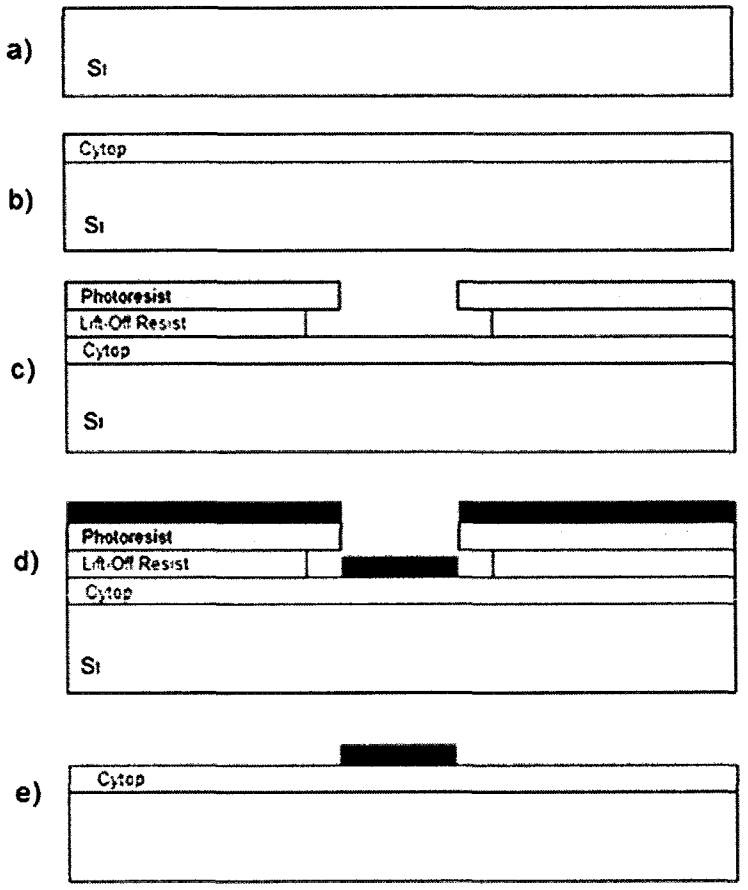

Figure 2: Flow of fabrication process.

The second step of the fabrication process (Table 1) consists of the spin-coat and cure of Cytop. Through experimentation, the processes described in Tables 2 and 3 (and discussed

further in the next section) were found to produce a thick, high quality layer of Cytop having a low surface roughness and a repeatable index of refraction.

The third step of the fabrication process (Table 1) consists of an ashing treatment applied to the Cytop surface in order to promote adhesion of the photolithography chemistry.

The final steps (4-6) of the fabrication process (Table 1) consist of applying the bi-layer lift-off lithography and metal deposition processes described in detail in Table 4 (and discussed further in the next section); this lithography process is a variation of that described in [21].

3. Process details and intermediate results

3.1 Cytop lower cladding

The first recipe attempted for depositing and curing Cytop was that suggested in the Cytop manual [24], executed as follows: i) spin-coat Cytop layer (spin speed determines thickness), ii) evaporate solvent at 80 °C for 60 minutes on a hot plate, iii) cure Cytop at 180 °C for 60 minutes. When following this recipe we noticed small holes uniformly distributed across the surface of the Cytop layer. Furthermore, the index of the layer when measured using a Metricon prism-coupler [32] was not as quoted in the Cytop specifications [24]. (The Metricon prism-coupler is used to measure both the thickness and the TE or TM refractive index of dielectric films.) After further investigation, we determined that the holes were caused by non-evaporated solvent left over from step ii) of the suggested process, and subsequently released during step iii) due to the higher temperature.

Through experimentation, the modified Cytop cure process described in Table 2 was found to be adequate. With this process, the presence of holes decreased and the index of refraction measured using the Metricon gave results which agreed better with the specifications

and were repeatable over many wafers. In order to deposit a thick layer of Cytop, a multi-spin coat/cure process was used, that is, steps 1 and 2 of Table 2 (using spin speed to adjust thickness) were repeated until the desired thickness was reached and then steps 3 and 4 were performed to cure the Cytop.

Step	Description	Details
1	Spin-coat	Spin speed depends on thickness desired and Cytop dilution
2	Solvent evaporation bake	Hot plate, 30 min @ 70 °C
Repeat Steps 1 and 2 to reach desired thickness		
3	Ramp temperature	Hot plate, ramp temperature from 70 °C to 250 °C over 180 min
4	Cytop cure bake	Hot plate, 60 min @ 250 °C

Table 2: Single and multi-layer Cytop cure process

A smooth flat Cytop surface upon which the Au stripes will be deposited is required. Generally, a high spin speed generates such a surface, but we found that spinning a 9% Cytop layer at spin speeds greater than 5000 rpm resulted in some unexpected defects in the film such as streak marks and a noticeable non-uniformity in thickness across the wafer. Spinning at a lower speed was found to be necessary. Also, diluting the Cytop solution to a 5% Cytop concentration using the supplied CT-SOLV180 solvent and spinning below 2000 rpm effectively eliminated the streaking effects observed with the faster spin.

Layer	Spin Rate (rpm) 10 s / 30 s	Cytop %
1 - 4	500/1000	9
5 - 7	500/2000	5

Table 3: Multi-layer Cytop spin-coat process

The Cytop spin-coat process described in Table 3 (in conjunction with the cure process in Table 2) was found to be suitable. This process produces four layers using 9% Cytop for the bulk

of the thickness, followed by three layers using 5% Cytop to ensure a smooth surface for metal deposition. The four layers of 9% Cytop were spun initially at 500 rpm for 10 s, then at 1000 rpm for 30 s, and each layer had a thickness of approximately 1.85 μm. The three layers of 5% Cytop were spun initially at 500 rpm for 30s, then at 2000 rpm for 30 s, and each layer had a thickness of approximately 0.2 μm. The total thickness of the stack was approximately 8 μm.

Step	Description	Details
1	Hexamethyl disiloxane deposition	Spin coat
2	Soft bake	Hot plate, 110 °C for 60 s
3	Lift-off resist deposition	Microchem LOR1A, spin coated at 1000 rpm for 10 s, then at 4000 rpm for 30 s
4	Soft bake	Hot plate, 110 °C for 60 s.
5	Positive photoresist deposition	Shipley S1805, spin coated at 1000 rpm for 10 s, then at 4000 rpm for 30 s
6	Soft bake	Hot plate, 110 °C for 60 s
7	Exposure	Karl Suss MA 6 contact mask aligner
8	Development	MF 321 solution (100%), 45 s develop time, static (no agitation), wafer is vertical
9	Rinse	15 s in de-ionized H_2O with light manual agitation, followed by static 60 s in a fresh de-ionized H_2O bath
10	Hard bake	Hot plate, 110 °C for 3 min
11	Metal deposition	E-beam evaporation, low deposition rate
12	Lift-off	10 min static dip in bath of Microposit 1165 at 65 °C, followed by 10 s ultrasonic treatment in this bath. Repeat in bath of fresh Microposit 1165.
13	Clean	Static dips in acetone and isopropyl alcohol each for 5 min or more depending on residue observed.

Table 4: Metal waveguide lift-off lithography process

Table 5 shows the index of refraction and thickness of thick Cytop layers fabricated in this manner (Tables 2 and 3), and measured using our Metricon prism coupler. SD% in Table 5 is the percentage of standard deviation of the measurement as calculated by the Metricon mode analysis software. It was difficult to achieve accurate TM measurements as evidenced by the

large standard deviations obtained in the results, especially at longer wavelengths (λ_0 = 1548 nm). This is thought to be caused by the TM modes of the (low-index) Cytop layer being too radiative into the underlying (high-index) Si substrate. The TE results are evidently more accurate (lower SD%). The TE refractive indices measured at λ_0 = 632.8, 1312 and 1548 nm are η_2 = 1.3399, 1.3359 and 1.3340, respectively. The indices are slightly higher than those listed in the manufacturer's specifications at essentially the same wavelengths [24] η_2 = 1.3395, 1.3348 and 1.3335, respectively. This may be due to different Cytop grades being used in these measurements. The thickness of the Cytop layer on both wafers is approximately 8 μm.

Thick Cytop Wafer #	**Measurement polarisation**	**Measurement wavelength (nm)**	**Refractive Index**	**SD%**	**Thickness d (μm)**	**SD%**
Cytop_147	TE	632.8	1.3399	0.00	7.9010	0.48
	TM	632.8	1.3399	0.00	7.7240	3.07
	TE	1312	1.3359	0.00	7.7954	0.18
	TM	1312	1.3355	0.01	7.8703	2.67
CT_REF	TE	632.8	1.3398	0.00	8.2769	0.22
	TM	632.8	1.3398	0.00	8.1463	1.69
	TE	1548	1.3340	0.00	8.2726	0.51
	TM	1548	1.3351	0.12	7.3633	17.19

Table 5: Index of refraction and thickness measurements of thick Cytop lower cladding

3.2 Bi-layer lift-off lithography

The third step of the fabrication process (Table 1) consists of a 5 s ashing of the Cytop surface in an O_2 plasma etcher to slightly roughen the surface in order to promote adhesion of the photolithography chemistry. Although the added roughness is undesirable, it was deemed necessary because of the difficulty we encountered with the adhesion of the photolithography

chemistry on a fresh (hydrophobic) Cytop surface. The ashing time was kept to a minimum in order minimize the roughness (as verified in section 4) while still having good adhesion.

Two problems were encountered with the Cytop when applying the nominal lift-off process described in [21]. (i) The first problem was the direct result of the descum step described therein, normally carried out after the hard bake (step 10, Table 4), and performed in an O_2 plasma etcher (45 s at a power of 100 W and a pressure of 0.3 Torr). The O_2 plasma etcher etched the exposed Cytop, opening trenches such that the Au stripes were deposited beneath the Cytop surface. Fig. 3(a) shows an AFM scan of an etched trench in the Cytop after Au deposition; it can be seen from this figure that the Au surface is approximately 129 nm below the surface of the surrounding Cytop. This problem was solved by eliminating the descum step, which is normally applied to remove excess debris from inside the opened channels that might be left over from developing. After optimising the lithography exposure time (as described below), it was determined through microscope inspections that very little to no debris was present inside the opened channels after developing. (ii) The second problem seemed to occur during the lift-off step of the nominal lithography process [21]. Fig. 3(b) shows an AFM scan of a pair of trenches in the Cytop approximately 19 nm deep on either side of an Au stripe. These trenches coincide with the edges of the metal stripe, which suggests that they are formed after metal deposition, and the only major process step after metal deposition is lift-off. This problem was overcome by decreasing the time the wafers were exposed to lift-off, to two 10 minute baths (step 12, Table 4) from two 20 minute baths in the nominal process [21]. The process steps described in Table 4 include these two modifications.

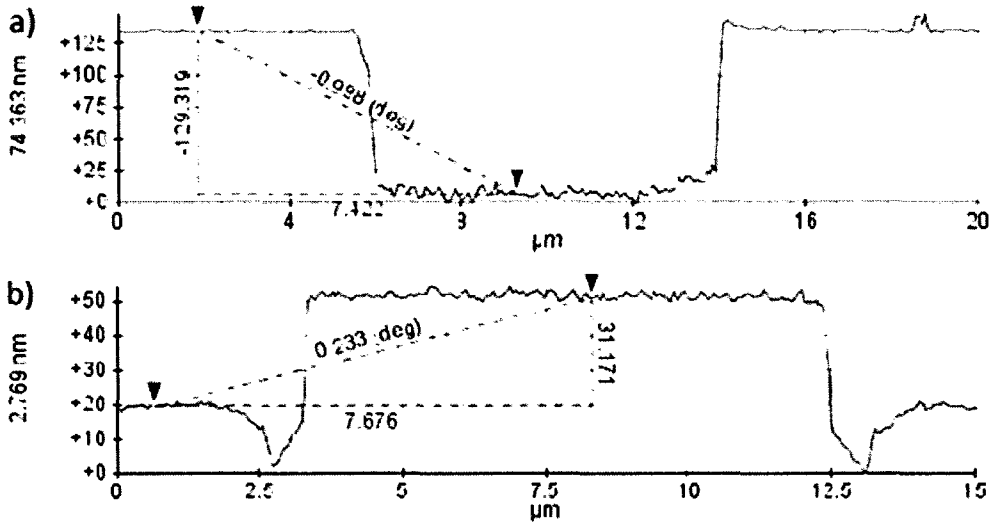

Figure 3: AFM measurement of a) etched trench and b) side trenches in Cytop.

A series of exposure time tests was conducted on our Karl-Suss MA6 mask aligner in order to determine the optimal exposure time required to achieve high quality lift-off following steps 1 to 10 of Table 4 (in the absence of a descum step and a shortened lift-off step). Fig. 4 shows a series of microscope images of the tests showing the quality of the lift-off photoresist at various exposure times. Fig. 4(a) shows an area of underexposed photoresist with an exposure time of 6 s; an abundance of leftover residue from developing is clearly visible (as pointed out by arrows). Fig. 4(b) shows an area of overexposed photoresist with an exposure time of 9 s; regions where the lift-off resist has lost adhesion to the Cytop are seen clearly (as pointed out by the arrow). Fig. 4(c) and Fig. 4(d) show areas of higher quality lift-off lithography where neither of these defects is visible; exposure times were 7 and 8 s, respectively. Using these results a final exposure time of 7.5 s was chosen.

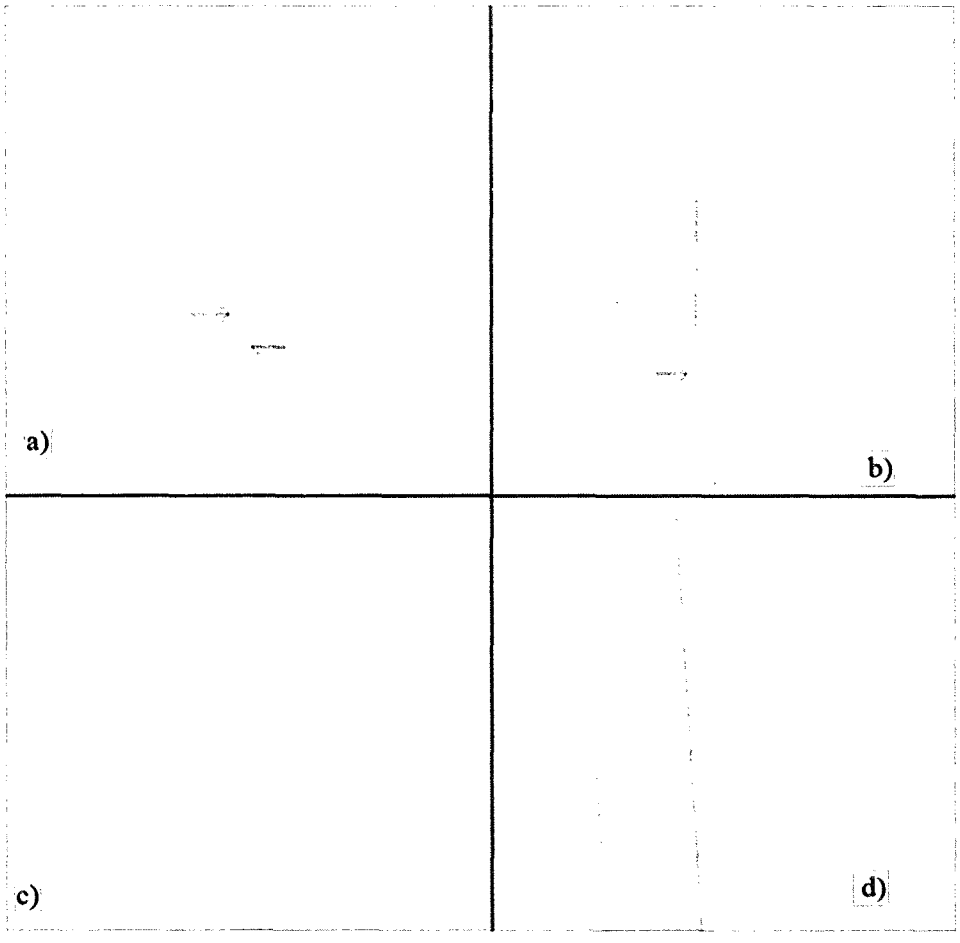

Figure 4: Microscope images of lithographic features as a function of exposure time: a) 6 s, 20× magnification; b) 9 s, 5× magnification; c) 7 s, 20× magnification; and d) 8 s, 50× magnification.

Fig. 5 shows a series of SEM images of the overhang achieved using this bi-layer lift-off lithography process; in each image the scale bar represents 1 μm.

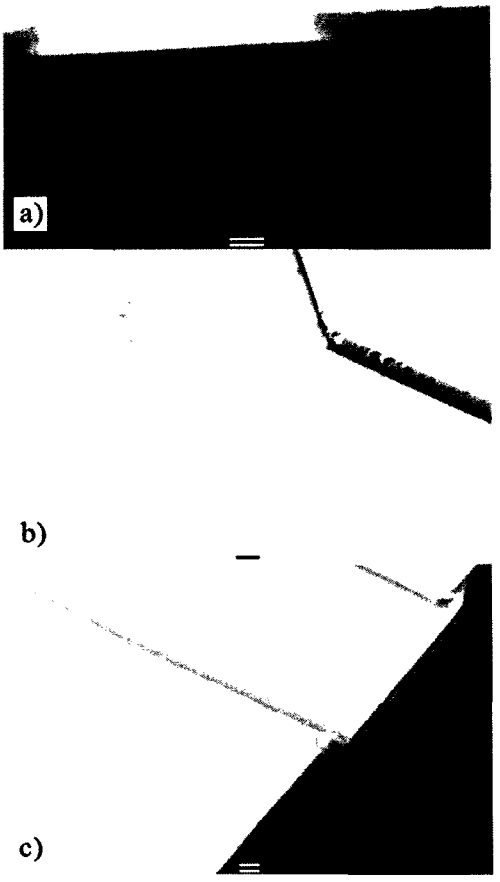

Figure 5: SEM images in different views (a) - (c) showing the overhang achieved using the bi-layer lift-off lithography process described in Table 4; the scale bar is 1 μm long in each case.

3.3 Metal deposition

Au was deposited at a low deposition rate of approximately 10 Å/sec using a Balzers BA510 e-beam evaporation system. The thickness was monitored during deposition using a quartz crystal, which oscillates at a resonance frequency that is dependent on the thickness and mass of the film deposited onto it. A series of deposition and lift-off runs were necessary to calibrate the evaporator, with AFM thickness measurements of Au stripes used as reference. Based on the AFM measurements it was determined that a tooling factor setting of 160% was

needed in order to achieve the target film thickness (the tooling factor is used to calibrate the crystal monitor to its position in the evaporation chamber relative to the deposition surface).

4. Finished Devices – wafer CT4

4.1 Physical characterisation

Finished devices were created on a wafer identified as CT4 by integrating all of the process steps described in Tables 1-4, with the exception that two additional layers of diluted 5% Cytop were added yielding a measured (Metricon) lower cladding thickness of d ~ 8.4 μm.

Fig. 6 shows low- and high-magnification microscope images of high-quality finished structures. Fig. 6(a) shows alternating Mach-Zehnder interferometers and straight waveguides, and Fig. 6(b) shows similar structures but having optically non-invasive electrical contacts. Figs. 6(c) and 6(d) show high-magnification images of a triple waveguide coupler and Y-junction with a contact arm and pad, respectively.

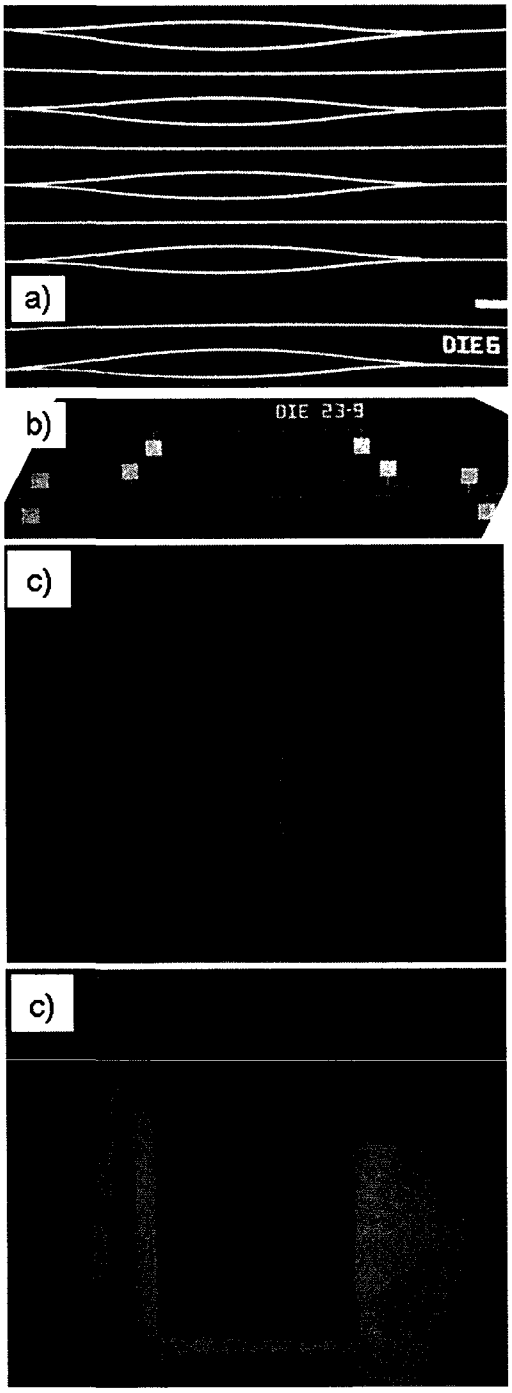

Figure 6: Microscope images of various integrated structures: (a) Mach-Zehnder interferometers and straight waveguides (low magnification); (b) Electrically contacted straight waveguide and Mach-Zehnder interferometer (low magnification); (c) triple waveguide coupler (100× magnification); (d) Y-junction with contact arm and pad (100× magnification).

Fig. 7 gives AFM scans of a short gap designed into an Au stripe. Such gaps are introduced into electrically contacted structures, such as those shown in Fig. 6(b), for the purposes of isolating electrically different parts of the structure. The line scans of Figs. 7(b) and 7(c) are taken across the top and bottom stripes of Fig. 7(a), respectively, revealing that the stripe width and thickness are w = 5.5 μm and t = 36 nm. Inspection of the scans also reveals that the gap length is 1.6 μm. The nominal (layout) stripe width and gap length are 5 and 2 μm, respectively, so the achieved stripe width is 10% larger than expected making the gap length 20% shorter. The stripe ends are rounded instead of square (as on the layout) due to resolution limitations, and the stripe width varies slightly along its length. These imperfections are not expected to compromise significantly the operation of the structures but they do underscore the need for further optimization of the lithography process. On the other hand, the measured Au thickness (36 nm) is very close to the nominal value (35 nm), and there is no evidence from these scans that the lift-off step (step 12, Table 4) has damaged the Cytop surface near the stripes. AFM measurements of other structures produced comparable results with the measured Au thickness ranging from 32 to 36 nm from structure to structure.

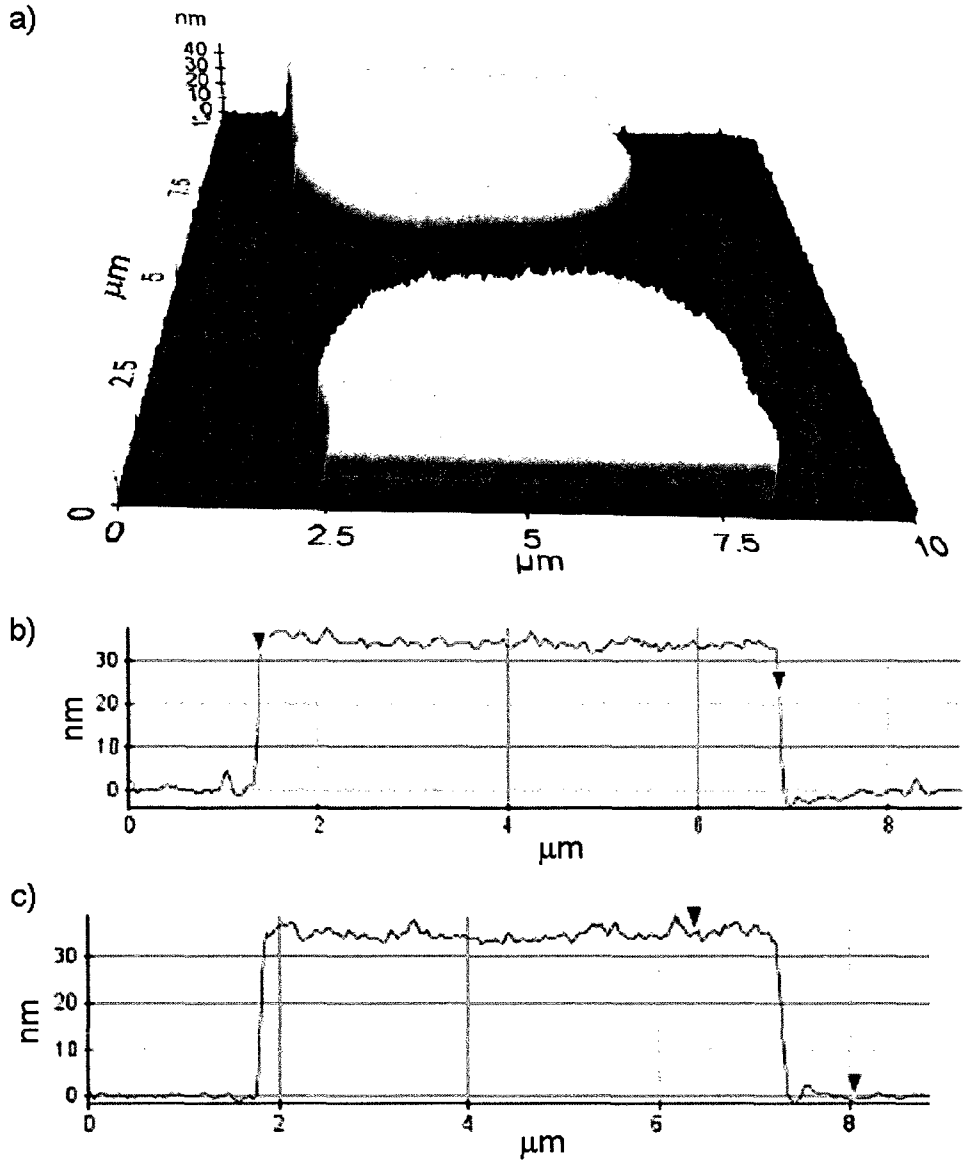

Figure 7: AFM scans of a gap between two Au stripes. (a) Surface scan of the gap region, (b) line scan across the top stripe, and (c) line scan across the bottom stripe.

Fig. 8 shows roughness scans of regions near the gap of Fig. 7(a); Fig. 8(a) shows a scan of the Cytop surface and Fig. 8(b) shows a scan of the top surface of one of the Au stripes. The Cytop surface has an rms roughness of 0.683 nm and an average roughness of 0.441 nm, whereas the Au stripe has an rms roughness of 0.917 nm and an average roughness of 0.694 nm. These

values are all below the desired maximum roughness of 1 nm; this maximum roughness minimizes light scattering. Any roughness added by the 5 s ashing step (step 3, Table 1) is evidently insignificant and optically irrelevant.

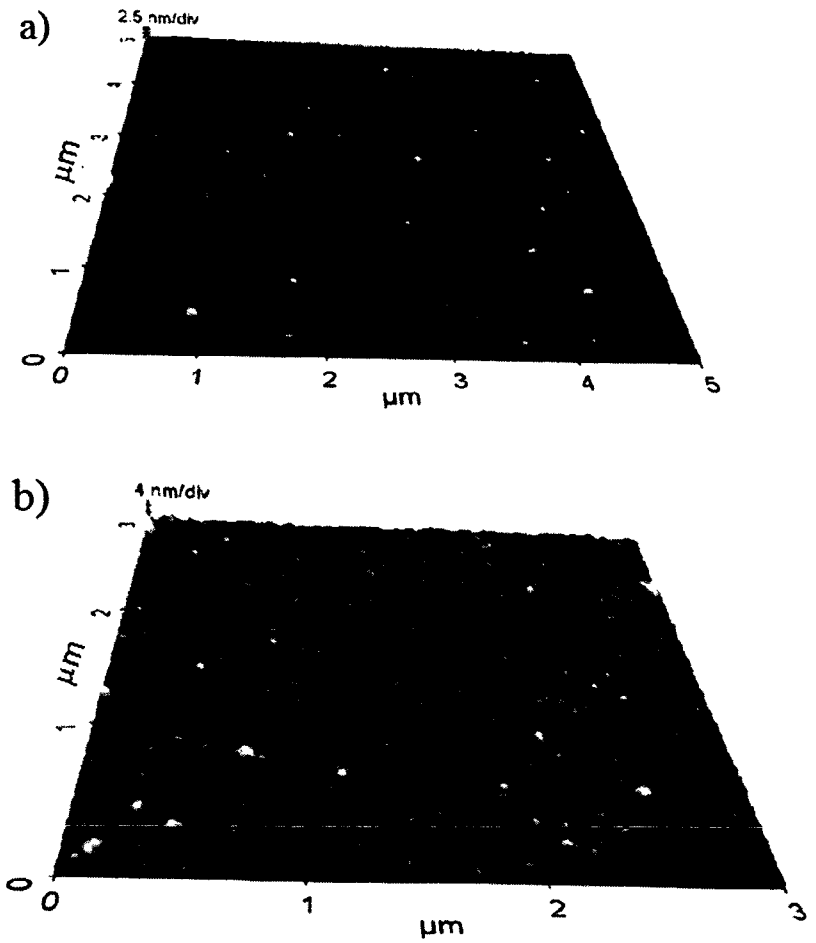

Figure 8: AFM surface roughness scans of regions near the gap of Fig. 7; a) Cytop surface and b) top surface of one of the Au stripes.

4.2 Defects

Y-junctions are important components of a Mach-Zehnder interferometer, and although most realised structures are of high quality, some occasionally exhibit defects, such as the one characterised by AFM in Fig. 9. Fig. 9(a) gives a surface scan of the junction region, Fig. 9(b) gives a line scan across the junction crotch, and Fig. 9(c) gives a line scan across the junction input. A few defects are apparent from Fig. 9(a), such as two metal bumps - one near the centre of the left output stripe and the other near the centre of the input stripe - which are due to evaporation "spits", and a metal "wing" along the left edge of the right output stripe near the crotch region likely due to poor lithography overhang in this region. Slight non-uniformities in the width of the stripes are also noted. Fig. 9(a) reveals a defect at the crotch in the form of a small metallic triangular feature instead of a nominal 1 μm flat spacing between the output stripes (as per the layout and as shown in Fig. 6(c)); the line scan of Fig. 9(b) shows this triangular feature to be of the same thickness as the stripes on either side. Figs. 9(b) and 9(c) reveal another problem in that the Cytop surface is sloped on the right side of the junction, rising ~10 nm over ~8 μm. The origin of this slope is unknown; we cannot rule out the lift-off step (step 12, Table 4) as being the cause. Except for the evaporation spits all of these defects can be corrected by further improvements in the lithography/lift-off processes. Such defects were noted on only a few Y-junctions, with the majority of the structures being of better quality.

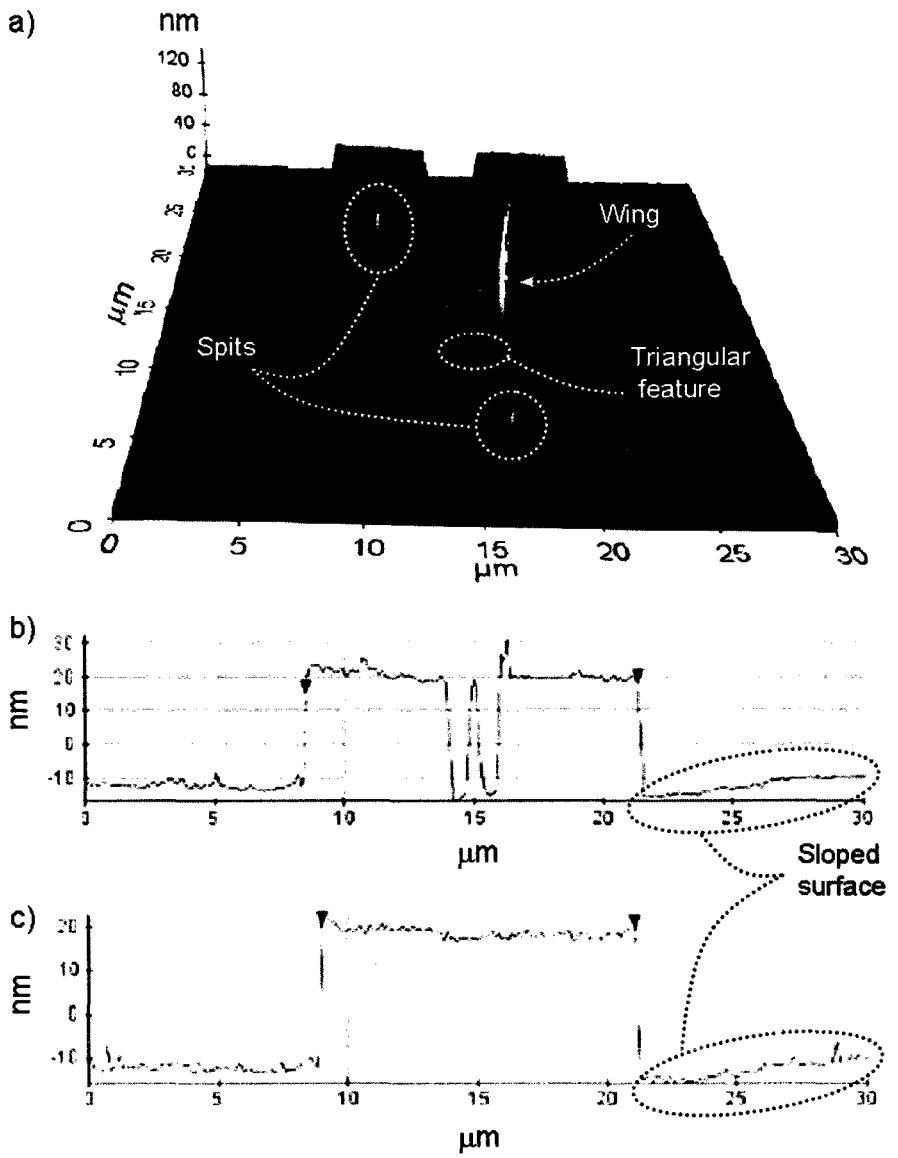

Figure 9: AFM scans of a Y-junction having defects. (a) Surface scan of the junction region, (b) line scan across the junction at the crotch, and (c) line scan across the junction input.

4.3 End facets

Cured Cytop of the grade selected (CTL-809M) was found to be malleable and soft. When wafers were cleaved at room temperature, the Cytop would stretch and eventually tear along the cleave plane, producing poor quality end facets. Freezing the wafer to harden the Cytop prior to cleaving improved the quality somewhat. Two methods were used to freeze the

wafer, the first was using a typical freezer at a temperature of approximately -20°C and the second was using liquid nitrogen at a temperature of approximately -196°C. Figs. 10(a) and 10(b) show SEM images of end facets of die cleaved from wafer CT4 using the first method of freezing; some deformation of the end facets is apparent from these images. From Fig. 10(b), the Cytop cladding thickness is noted to be d ≅ 8.4 μm, in good agreement with the Metricon measurement.

Dicing the wafers, while protecting the metal stripes with photoresist, produced significantly improved end facets.

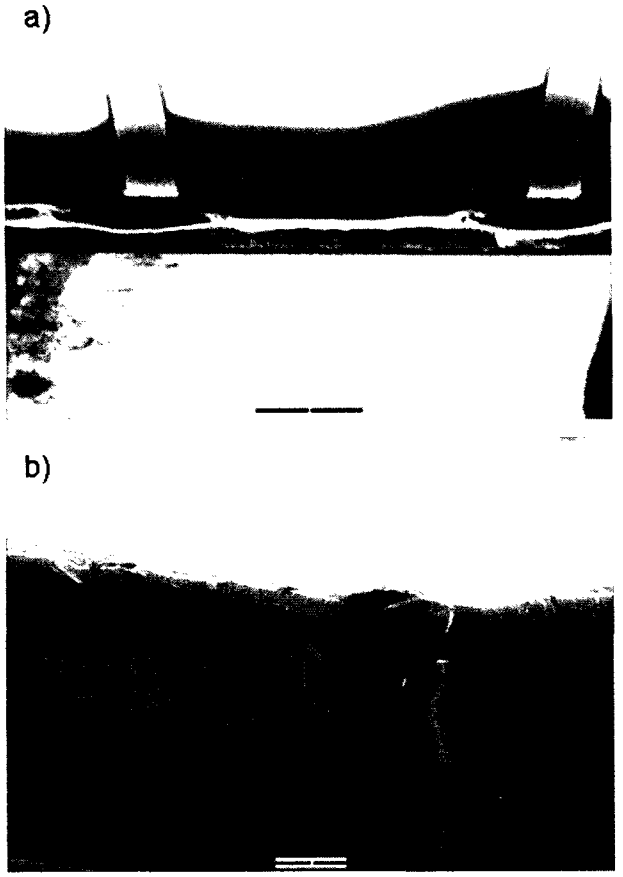

Figure 10: (a) and (b) SEM images of unpolished end facets of cleaved die; the scale bar on the images represents 10 μm. (b) d ≅ 8.4 μm thick Cytop cladding on Silicon; the arrow identifies the Cytop/Si interface.

4.4 Optical Measurements

The full process described in Table 1 produced working waveguides as confirmed by observing an infrared image of an LRSPP mode output, as shown in Fig. 11, from an approximately 5 mm long straight waveguide (with cleaved end facets). The waveguide was excited at λ_0 = 1310 nm with Cargille oil (η_1=1.335) as the index matching environment on top of the stripe and polarisation-maintaining single-mode fiber butt-coupled to the input [9]. The Cargille oil was eventually absorbed by the Cytop cladding ultimately destroying the waveguide (it was subsequently found that the Cargille oil has as a constituent part the same solvent that is used to dissolve Cytop) - no such problems were observed with aqueous solutions used as the upper cladding [29]. The mode power attenuation of the LRSPP was measured for three straight identical waveguides, yielding an average attenuation of 7.43 dB/mm, in very good agreement with theoretical predictions [29].

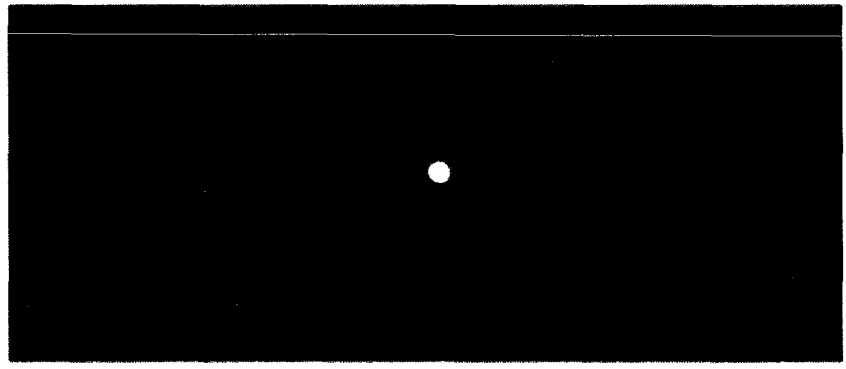

Figure 11: Infrared image of the LRSPP mode output from a straight waveguide.

5. Summary and concluding remarks

The process flow and physical characterisation of thin metal stripe waveguides and integrated components suitable for propagating LRSPPs on an optically infinite (> 8 μm) Cytop layer were described. The thick Cytop layer was created using a multilayer spin-coat/cure recipe resulting in a layer of Cytop approximately 8.4 μm thick. The thin Au stripe waveguides were deposited using e-beam evaporation and defined with a bi-layer lift-off photoresist process; the Au stripes are 32 to 36 nm thick and 5.5 μm wide.

Physical characterizations of devices at various stages of fabrication were conducted in order to create a repeatable process capable of yielding consistent waveguide dimensions. Physical characterization of finished devices was also conducted and the results were discussed. Optical microscope, SEM and AFM inspections, and Metricon measurements, were used to characterize the devices. Finished device structures include straight waveguides, Y-junctions, Mach-Zehnders and couplers. Working waveguides were demonstrated by observing an infrared image of the LRSPP mode output.

Issues with some of the process steps were encountered during fabrication, including pinholes in the Cytop layer after curing, etched Cytop trenches due to O_2 plasma descum, and etched Cytop trenches at the edges of the Au stripes due to the lift-off baths. Solutions to these problems were found and presented.

6. Acknowledgements

The author gratefully acknowledges Robin Buckley (University of Ottawa) for conducting the simulations, Ewa Lisicka-Skrzek (University of Ottawa) for help with the optical experiments, Heng-Yong Nie of Surface Science Western for conducting the AFM

measurements, and Norman Fong, Rob Vandusen and Carol Adams (Carleton University) for assistance with the fabrication.

References

[1] W. L. Barnes, J. Opt. A 8 (2006) S87.

[2] W. L. Barnes, A. Dereux, and T. W. Ebbesen, Nature 424 (2003) 824.

[3] S. A. Maier and H. A. Atwater, J. Appl. Phys. 98 (2005) 011101.

[4] P. Berini, Phys. Rev. B 61 (2000) 10484.

[5] P. Berini, Phys. Rev. B 63 (2001) 125417.

[6] J. C. Weeber, A. Dereux, C. Girard, J. R. Krenn, and J. P. Goudonnet, Phys. Rev. B 60 (1999) 9061.

[7] R. Charbonneau, P. Berini, E. Berolo, and E. Lisicka-Shrzek, Opt. Lett. 25 (2000) 844.

[8] R. Nikolajsen, K. Leosson, I. Salakhutdinov, and S. I. Bozhevolnyi, Appl. Phys. Lett. 82 (2003) 668.

[9] P. Berini, R. Charbonneau, N. Lahoud, and G. Mattiussi, J. Appl. Phys. 98 (2005) 043109.

[10] A. Boltasseva, T. Nikolajsen, K. Leosson, K. Kjaer, M. S. Larsen, and S. I. Bozhevolnyi, J. Light. Technol. 23 (2005) 413.

[11] R. Charbonneau, C. Scales, I. Breukelaar, S. Fafard, N. Lahoud, G. Mattiussi, and P. Berini, J. Light. Technol. 24 (2006) 477.

[12] A. Degiron, S.-Y. Cho, T. Tyler, N. M. Jokerst, and D. R. Smith, New J. Phys. 11 (2009) 015002.

[13] H. S. Won, K. C. Kim, S. H. Song, C.-H. Oh, P. S. Kim, S. Park, and S. I. Kim, Appl. Phys. Lett. 88 (2006) 011110

[14] P. Berini, New J. Phys. 10 (2008) 105010.

[15] A. W. Wark, H. J. Lee, R. M. Corn, Anal. Chem. 77 (2005) 3904.

[16] A. Kasry and W. Knoll, App. Phys. Lett. 89 (2006) 101106.

[17] R. Slavík and J. Homola, Sens. Act. B 123 (2007) 10.

[18] J. Dostálek, A. Kasry, and W. Knoll, Plasmonics 2 (2007) 97.

[19] R. Charbonneau, M. Tencer, N. Lahoud, and P. Berini, Sens. Act. B 134 (2008) 455.

[20] P. Berini, R. Charbonneau, and N. Lahoud, Nano Lett. 7 (2007) 1376.

[21] P. Berini, N. Lahoud and R. Charbonneau, J. Vac. Sci. Technol. A 26 (2008) 1383.

[22] D. J. Segelstein, M.Sc. Thesis, University of Missouri, Kansas City, 1981.

[23] Dupont, "Teflon AF Properties", http://www.dupont.com/

[24] Asahi Glass Company, "Technical Information Cytop", distributed by Bellex International Corporation, http://www.bellexinternational.com/

[25] Y.-G. Zhao, W.-K. Lu, Y. Ma, S.-S. Kim, S. T. Ho, and T. J. Marks, Appl. Phys. Lett. 77 (2000) 2961

[26] Y. Kuwana, S. Takenobu, K. Takayama, and Y. Morizawa, Rep. Res. Lab. Asahi Glass Co. Ltd. 56 (2006) 35

[27] Y. Matsumoto, K. Yoshida, M. Ishida, Sens. Act. A 66 (1998) 308

[28] C. H. Lin, F. K. Oshita, M. J. Jennison, P. C. Chang, J. Wei, C. Wilhelmi, M. Bramlett, R. Parkhurst, S. D. Strathman, M. Maple, Solid-State Electr. 49 (2005) 1708

[29] R. Daviau, E. Lisicka-Skrzek, R. N. Tait, and P. Berini, "Broadside excitation of surface plasmon waveguides on Cytop", Appl. Phys. Lett., in press

[30] *Handbook of Optical Constants of Solids*, edited by E. D. Palik (Academic, Orlando, FL, 1985).

[31] A. Ribner, Plasmatic Systems, Inc.

[32] Metricon Corporation, Metricon Model 2010/M http://www.metricon.com

Chapter 3

Broadside excitation of surface plasmon waveguides on Cytop

Preamble

The paper presents mode power attenuation measurements for the waveguides fabricated in Chapter 2. The waveguides were tested using a broadside coupling technique whereby tapered single-mode fibres are positioned in direct contact with the metal stripe such that the slow mode of the fibre couples through partial modal overlap to the long-range surface plasmon.

Contributions

The authors are grateful to Michal Tencer and Federico Carvajal for assistance with the preparation and characterisation of the buffer solution and Ewa Lisicka-Skrzek for help with the optical experiments.

Broadside excitation of surface plasmon waveguides on Cytop

Richard Daviau,[1] Ewa Lisicka-Skrzek,[1] R. Niall Tait,[2] and Pierre Berini[1,3,4,a)]
[1]*School of Information Technology and Engineering, University of Ottawa, 161 Louis Pasteur St., Ottawa, Ontario K1N 6N5, Canada*
[2]*Department of Electronics, Carleton University, 1125 Colonel By Drive, Ottawa, Ontario K1S 5B6, Canada*
[3]*Department of Physics, University of Ottawa, 150 Louis Pasteur St., Ottawa, Ontario K1N 6N5, Canada*
[4]*Spectalis Corp., P.O. Box 72029, Kanata North RPO, Ottawa, Ontario K2K 2P4, Canada*

(Received 19 January 2009; accepted 1 February 2009; published online 5 March 2009)

Long-range surface plasmon waveguides consisting of a Au stripe on Cytop, covered with an index-matched aqueous solution, are described and characterized. The waveguides are tested using a broadside coupling technique, whereby tapered single-mode fibers are positioned in direct contact with the stripe such that the slow mode of the fiber couples through partial modal overlap to the long-range surface plasmon. Attenuation measurements obtained at λ_0=1310 nm agree well with theory, thus validating the waveguide fabrication and experimental techniques. The waveguides are useful for (bio)chemical sensing and the broadside coupling technique is useful for on-wafer optical probing. © *2009 American Institute of Physics*. [DOI: 10.1063/1.3093500]

Surface plasmon polaritons are transverse magnetic (TM) polarized optical surface waves that propagate along the interface between a metal and a dielectric.[1] The symmetrically cladded thin metal stripe[2] supports as a fundamental mode, a long-range (low-loss) surface plasmon-polariton (LRSPP) wave denoted the ss_b^0 mode. This waveguide and the LRSPP propagating therealong are promising for (bio)chemical sensing given the favorable trade-off between modal sensitivity (bulk and surface) and attenuation that is achievable,[3] and the ability to create integrated long interaction length structures such as guided-wave Mach–Zehnder interferometers. For sensing applications, a symmetric refractive index involving the sensing medium can be achieved by supporting the metal stripe with an optically not-too-invasive freestanding dielectric membrane and allowing the sensing medium to surround the stripe.[4] Alternatively, a thick lower cladding, index matched to the sensing medium above the stripe, can be used if a suitable lower cladding material is available. In the case of biochemical sensors, the sensing medium is typically an aqueous solution so low-index polymers such as Cytop[5] and Teflon AF (Ref. 6) could be used as the lower cladding. Compared to a supporting membrane[4] this approach is simpler, but it requires that the index of the sensing medium remains matched to that of the lower cladding to within about 10^{-3}.

The LRSPP has been excited via prism coupling on a thin metal slab cladded with Cytop or Teflon on one side and exposed to an aqueous sensing medium on the other side.[7–10] In this letter we describe the excitation of the LRSPP along thin Au stripes (i.e., low-loss ss_b^0 mode[2]) on Cytop covered with an index-matched aqueous buffer, and we give attenuation measurements for the mode at a free-space operating wavelength of λ_0=1310 nm. A broadside fiber coupling technique using tapered fibers was devised to excite the waveguides and is also described.

The waveguide of interest is sketched in Fig. 1 and consists of a Au stripe of thickness t, width w, and permittivity ε_1, on an optically infinite lower cladding of Cytop of thickness d and permittivity ε_2, covered by an aqueous solution of permittivity ε_3. The structures were fabricated by spin coating and curing Cytop on a Si substrate and by Au evaporation (no adhesion layer) and lift-off, as described in detail elsewhere.[11]

A popular technique for exciting waveguide modes is end-fire excitation (butt coupling). This technique has been shown to efficiently excite the LRSPP in straight symmetrically cladded thin metal stripes[12–14] and associated passive elements,[15,16] including the metal stripe on Cytop.[11] However, access to good quality end facets is required for end-fire

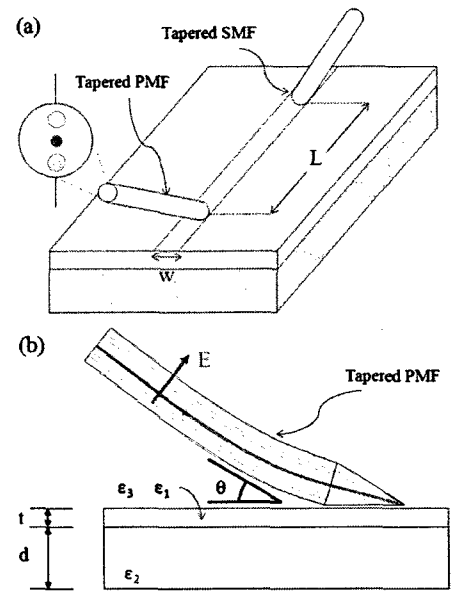

FIG. 1. (Color online) (a) Sketch of a straight metal stripe on an optically infinite layer of Cytop (light gray) and on a Si substrate (dark gray). A tapered PMF is used to excite the waveguide at broadside by partial mode overlap. A sketch of its input facet shows its core and stress members as the light blue and gray dots, and the orientation of its slow axis with the vertical lines. A tapered SMF is used to capture the output light at a distance L from the input tapered PMF. (b) Sagittal plane near the launch point, through the center of the tapered PMF and the metal stripe waveguide.

a)Author to whom correspondence should be addressed. FAX: (613) 562-5175. Electronic mail: berini@site.uottawa.ca.

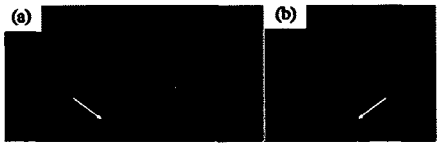

FIG. 2. Infrared images of output modes (a) before thermal tuning and (b) after thermal tuning.

excitation, precluding its use for optical wafer probing. An alternative technique is prism coupling along the top surface of the waveguide, as applied to excite the LRSPP in metal slabs[7–10] and stripes.[17] In prism coupling,[17] p-polarized light, incident at the base of a high-index prism beyond the critical angle, couples evanescently to the LRSPP of the waveguide when the spacing between the prism and the top surface of the waveguide is properly adjusted. Difficulties in applying this technique include controlling both the spacing and parallelism between the base of the prism and the waveguide, and ensuring that the angle of incidence of the input light is what is desired for optimal coupling, while ensuring that the permittivities of the upper and lower claddings remain closely matched.

Evanescent coupling using an angle-cleaved polarization-maintaining fiber (PMF) eliminates many of these difficulties[18] but requires a PMF cleaved or polished at a specific angle. The coupling scheme devised here is inspired from this technique[18] but replaces the angle-cleaved PMF with a tapered PMF. The coupling scheme is sketched in Fig. 1. A tapered Panda PMF (Ref. 19) was selected as the input fiber; the input facet of this PMF is sketched in enlarged view in Fig. 1(a), showing its core and stress members and identifying its slow axis. Figure 1(b) shows part of the sagittal plane near the launch point, taken through the center of the PMF and the metal stripe waveguide; the slow axis of the PMF is oriented in this plane. Polarized light is launched into the PMF so that only the slow mode is excited, sketched as the red arrow along the core of the PMF with the electric field (E) oriented as shown. The flat edge of the tapered PMF tip is positioned in contact at broadside to the metal stripe such that the slow mode of the PMF excites the LRSPP mode of the waveguide via partial modal overlap in a manner similar to end-fire excitation. The output power of the waveguide is measured by positioning the flat edge of a tapered single-mode fiber (SMF) in contact with the metal stripe at a distance L from the input PMF such that the LRSPP excites the fundamental mode of the SMF also through partial modal overlap. The top insets of Fig. 3 show microscope images of the tips of the input tapered PMF and the output tapered SMF used.

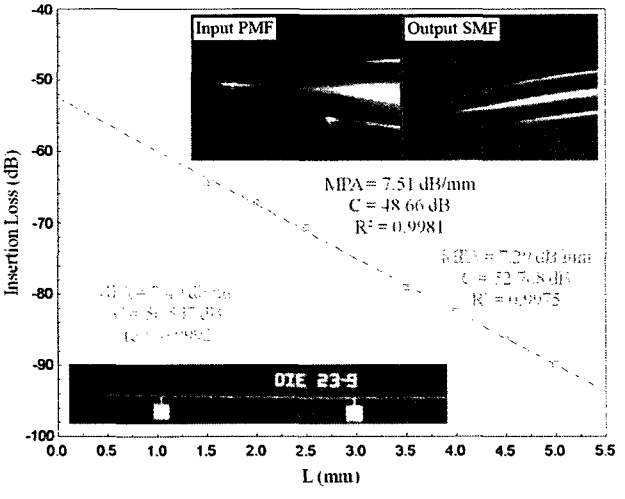

FIG. 3. (Color online) Insertion loss measurements of three different straight waveguides obtained using the setup sketched in Fig. 1 with the input tapered PMF in a fixed position and the output tapered SMF changing the separation distance L. The top inset shows microscope images of the tips of the input tapered PMF and the output tapered SMF. The bottom inset shows a microscope image of a typical straight waveguide (with electrical contact arms and pads).

The waveguides available for testing had a Au stripe of width $w=5.4$ μm, a thickness in the range of $t=32-36$ nm, and a roughness along the Au and Cytop surfaces below 1 nm (average and root mean square), as measured using atomic force microscopy.[11] The Cytop lower cladding thickness was $d=8.4$ μm thick and its TM relative permittivity was $\varepsilon_{r,2}=(1.3355)^2$ at $\lambda_0=1312$ nm, as measured using a Metricon system.[11,20] A microscope image of a typical fabricated straight waveguide is shown as the bottom inset in Fig. 3. The waveguide under test was immersed in index-matched buffer held at 26 °C in a thermally controlled basin. The index-matched buffer consisted of phosphate buffer with a nominal concentration of 0.6702M, having a relative permittivity of $\varepsilon_{r,3}=(1.3352)^2$ at $\lambda_0=1312$ nm, as measured using a Metricon system.[20] This buffer was prepared by diluting stock 1.0M phosphate buffer supplied by Sigma-Aldrich (Catalog No. P3619, pH=7.4), the density of which was measured to be 1.121 64 g/ml. Thus, 75.1723 g (67.02 ml) of stock buffer was topped up to 100 ml with de-ionized water to achieve the 0.6702M concentration desired for index matching.

The input PMF was aligned to the waveguide under test using optomechanical stages. Proper alignment was verified by observing the output mode with an infrared camera, as shown in Fig. 2(a) before thermal tuning and in Fig. 2(b) after thermal tuning. The tuning temperature (26 °C) was chosen to minimize the background light observed [cf. Fig. 2(a)] and to produce a nicely symmetric mode output [i.e., Fig. 2(b)], both conditions indicating accurate matching of the buffer and Cytop refractive indices.

The technique was then applied to generate cutback curves for three different straight metal stripe waveguides of the same design and taken from the same wafer by changing the separation distance L between the input PMF and output SMF and measuring the total insertion loss (including the losses of the fibers and connectors that are negligible). The input PMF was aligned and remained at a fixed position while the output SMF was moved along the waveguide to generate a set of data points. A minimum separation distance of approximately 1.5 mm between the input and output fibers was kept in order to ensure that any uncoupled stray radiation from the input fiber did not affect the measurements. The angle of the fibers relative to the horizontal axis [Fig. 1(b)] was set to $\theta\sim 18°$ (unoptimized). The cutback measurements at $\lambda_0=1310$ nm are plotted in Fig. 3. The slope gives the mode power attenuation (MPA) of the LRSPP and the intercept gives the total coupling losses (C). The measured MPAs are 7.51, 7.29, and 7.49 dB/mm, and the total coupling losses are $C=48.66$, 52.77, and 56.55 dB; the individual input and output coupling losses cannot be estimated because the PMF and SMF have different tapers (bottom left

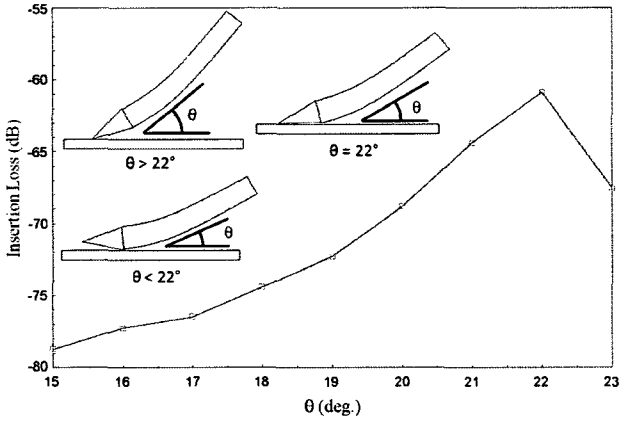

FIG. 4. (Color online) Insertion loss measurements of a straight waveguide obtained using the setup sketched in Fig. 1 with the input tapered PMF in a fixed position and the output tapered SMF at a fixed separation L but for different angles θ.

inset of Fig. 3). The R^2 goodness of fit[14] is better than 99% in all cases.

The MPA of the LRSPP was computed using the method of lines[2] at $\lambda_0=1310$ nm for this waveguide design, assuming the measured width of an Au stripe ($w=5.4$ μm) and the average measured thickness ($t=34$ nm), and the measured thickness and index of the Cytop cladding [$d=8.4$ μm and $\varepsilon_{r,2}=(1.3355)^2$].[11] The index of the underlying Si substrate was taken as[21] 3.5029, the relative permittivity of Au as[21] $\varepsilon_{r,1}=-86.08-j8.322$, and the index of the thermally matched buffer solution as $\varepsilon_{r,3}=(1.3355)^2-j2(1.3355)k$ with $k=1.639\times10^{-5}$ as the absorption coefficient of water at this wavelength.[22] The computed MPA is 7.1 dB/mm, which is very close to the measured MPAs.

The total coupling losses vary from 48.66 to 56.55 dB from waveguide to waveguide, a variation ascribed to differences in the fiber angles θ (the angles were kept constant during cutback but varied from one waveguide to another). Figure 4 plots the total insertion loss versus the angle θ of the output SMF with the input PMF remaining at a fixed angle. The optimal angle for the output SMF is $\theta\sim22°$, where the coupling loss is reduced by about 20 dB relative to the shallowest angle ($\theta=15°$). Also, there is a decrease in coupling loss of ~14 dB at $\theta=22°$ compared to $\theta=18°$ (the angle used for the measurements in Fig. 3), so the total coupling loss could be reduced by ~28 dB if both fibers were optimally angled, giving a total coupling loss of ~25 dB for the setup. This is high compared to end-fire coupling[14] but is good enough for optical wafer probing and for verifying the operation of structures. The sketches in the inset to Fig. 4 explain how the coupling loss varies with θ. The flat edge of the fibers must be in contact at broadside with the Au stripe to maximize the partial overlap with the LRSPP (and thus to minimize the coupling loss). A small pressure was applied to the fibers to achieve full contact, causing the fibers to bend slightly as depicted. At angles greater than, or less than, the optimal (22° in this case) only a small portion of the flat edge is in contact at broadside.

In summary, LRSPP waveguides consisting of a Au stripe on Cytop, and covered with an index-matched aqueous buffer, were characterized at $\lambda_0=1310$ nm. Additionally, a broadside modal overlap coupling technique using a tapered PMF was demonstrated by exciting the LRSPP and generating cutback curves. The Au stripes on Cytop are useful for biosensor applications, and the broadside coupling technique is useful for optical wafer probing.

The authors are grateful to Michal Tencer and Federico Carvajal for assistance with the preparation and characterization of the buffer solution.

[1]W. L. Barnes, J. Opt. A, Pure Appl. Opt. **8**, S87 (2006).
[2]P. Berini, Phys. Rev. B **61**, 10484 (2000).
[3]P. Berini, New J. Phys. **10**, 105010 (2008).
[4]P. Berini, R. Charbonneau, and N. Lahoud, Nano Lett. **7**, 1376 (2007).
[5]Asahi Glass Company, Technical Information Cytop, distributed by Bellex International Corporation (http://www.bellexinternational.com/).
[6]Dupont, Teflon® AF Properties (http://www.dupont.com/).
[7]A. W. Wark, H. J. Lee, and R. M. Corn, Anal. Chem. **77**, 3904 (2005).
[8]A. Kasry and W. Knoll, Appl. Phys. Lett. **89**, 101106 (2006).
[9]R. Slavík and J. Homola, Sens. Actuators B **123**, 10 (2007).
[10]J. Dostálek, A. Kasry, and W. Knoll, Plasmonics **2**, 97 (2007).
[11]R. Daviau, P. Berini, and R. N. Tait (unpublished).
[12]R. Charbonneau, P. Berini, E. Berolo, and E. Lisicka-Shrzek, Opt. Lett. **25**, 844 (2000).
[13]R. Nikolajsen, K. Leosson, I. Salakhutdinov, and S. I. Bozhevolnyi, Appl. Phys. Lett. **82**, 668 (2003).
[14]P. Berini, R. Charbonneau, N. Lahoud, and G. Mattiussi, J. Appl. Phys. **98**, 043109 (2005).
[15]R. Charbonneau, N. Lahoud, G. Mattiussi, and P. Berini, Opt. Express **13**, 977 (2005).
[16]A. Boltasseva, T. Nikolajsen, K. Leosson, K. Kjaer, M. S. Larsen, and S. I. Bozhevolnyi, J. Lightwave Technol. **23**, 413 (2005).
[17]R. Charbonneau and P. Berini, Rev. Sci. Instrum. **79**, 073106 (2008).
[18]R. Charbonneau, E. Lisicka-Shrzek, and P. Berini, Appl. Phys. Lett. **92**, 101102 (2008).
[19]Corning Inc. (www.corning.com).
[20]Metricon Corporation, Metricon model 2010/M (http://www.metricon.com).
[21]*Handbook of Optical Constants of Solids*, edited by E. D. Palik (Academic, Orlando, FL, 1985).
[22]D. J. Segelstein, M.S. thesis, University of Missouri, 1981.

Chapter 4

4.1 - Summary and Concluding Remarks

The fabrication of thin-film metal stripe surface Plasmon waveguides and integrated components on Cytop was carried out. The full process flow (Chapter 2, Table 1) was developed by optimizing and verifying through physical characterization each independent step before integrating them together as a full process. The second step of the process involved creating a thick layer of Cytop to be used as the bottom cladding and was done by using a multi layer spin-coat/cure process (Chapter 2, Table 2). The Cytop deposition step was considered to be optimized when the index (n=1.3355) and desired thickness (>8um) of the Cytop layer as measured by the Metricon was what was desired and able to be reproduced. The last three steps of the process (bi-layer metal lift-off lithography) were taken from a previously used recipe for creating metal stripe Plasmon waveguides and adapted to be used on Cytop. These lift-off lithography steps were considered to be optimized when three important parameters were met as measured by Atomic Force Microscope: a) sub-nanometre surface roughness for Au, b) Au stripe thickness to be approximately 35nm and c) Au stripe width to be approximately 5um.

Mode power attenuation measurements of the fabricated metal stripe Plasmon waveguides were made using a novel cutback technique. The technique involved using a tapered polarization maintaining fibre in direct contact with the broadside of an Au stripe to excite through partial modal overlap the long-range surface Plasmon-polariton mode of the waveguide. In order for the LRSPP to propagate a nearly symmetrical background index is required and so the device under test was submersed in a liquid buffer solution index matched to Cytop. The output power was measured using a tapered single mode fibre in direct contact with the Au stripe at various distances from the input fibre to

generate a cutback curve. The measured and computed attenuations of the LRSPP were in very good agreement.

The mode power attenuation measurements conclusively show that it is indeed possible to use Cytop as a low-index dielectric for a lower cladding of LRSPP waveguides. The very good agreement observed between the measured and theoretical attenuations indicate high quality fabrication. The excitation technique used for the MPA measurements to excite the LRSPP mode was found to be both successful and easy to implement. Although the coupling losses were found to be quite large, they can be lowered by a significant amount by optimizing the angle at which the tapered fibre makes contact with the broadside of the waveguide. The Cytop grade selected for this project was found to be malleable and soft thus inhibiting the creation of optically high quality end facets through cleaving and polishing needed for use with a more conventional coupling technique such as end-fire excitation.

4.2 - Suggestions for Future Work

The eventual goal of this waveguide architecture is for its use in (bio)chemical sensing. Since it was determined that Cytop can be used as a low-index dielectric material the next logical step is to create an upper Cytop cladding with flow cells, allowing testing of an integrated sensing structure. In this fully integrated structure it would be beneficial if waveguides could be excited using an end-fire coupling technique. This might be possible to achieve by changing the selected Cytop to the CTX grade which has a higher molecular weight and might be less malleable, allowing for optically higher quality end facets that can be polished.

4.3 – Thesis Contributions

The work accomplished with this thesis provides a solid starting point for the eventual goal of using this waveguide architecture for use in (bio)chemical sensing. It was shown that a thick layer of Cytop can be deposited and used as a low-index dielectric in supporting LRSPP waveguides. Additionally, a partial modal overlap excitation technique using a tapered polarization maintaining fibre was demonstrated.

APPENDIX A

SPP Field derivation

Figure 1-1 shows the orientation of the metal and dielectric regions, propagation is along the +z direction (out of the page) with $e^{-j\omega t}$ time dependency.

The relative permittivity of the metal region is given by $\varepsilon_{r,metal}$
The relative permittivity of the dielectric region is given by $\varepsilon_{r,dielectric}$

SPP modes are TM polarized waves and as such we begin our derivation by considering a tangential magnetic field in region i (metal or dielectric), and is given by the following equation

$$\overline{H_i} = \hat{x}H_0 e^{-(\alpha_{y,i})y} e^{-(\gamma_z)z} \tag{1}$$

Where γ_z is the complex propagation constant and is given by

$$\gamma_z = \alpha_z + j\beta z \tag{2}$$

We know that transverse magnetic fields are continuous across a perpendicular interface and as such H_0 is the same both the metal and dielectric regions.

Beginning with Maxwell's equations in differential form:

$$\nabla \times \overline{E} = -j\omega\mu\overline{H} + \overline{M} \tag{3}$$
$$\nabla \times \overline{H} = j\omega\mu\overline{E} + \overline{J} \tag{4}$$
$$\nabla \cdot \overline{E} = \rho/\epsilon \tag{5}$$
$$\nabla \cdot \overline{H} = 0 \tag{6}$$

Since we have a source free medium, the electric and magnetic current densities as well as the electric volume charge density, denoted as $\overline{M}$, $\overline{J}$ and ρ, respectively, are all equal to zero. Inserting this into the equations 3, 4 and 5 gives us:

$$\nabla \times \overline{E} = -j\omega\mu\overline{H} \tag{7}$$
$$\nabla \times \overline{H} = j\omega\mu\overline{E} \tag{8}$$
$$\nabla \cdot \overline{E} = 0 \tag{9}$$
$$\nabla \cdot \overline{H} = 0 \tag{10}$$

Using equation (8) we can find the electric field components of the TM mode in each of the media i, giving us:

$$\overline{E_i} = \frac{\hat{y}(j\gamma_z)}{\omega\epsilon_0\epsilon_{r,i}} H_0 e^{(-1)^i(\alpha_{y,i})y} e^{(-\gamma_z)z} + \frac{\hat{z}\left((-1)^i j\alpha_{y,i}\right)}{\omega\epsilon_0\epsilon_{r,i}} H_0 e^{(-1)^i(\alpha_{y,i})y} e^{(-\gamma_z)z} \tag{11}$$

The transverse wave number in the metal region, $\alpha_{y,metal}$, can be calculated by substituting (11) into (7) which gives us

$$\alpha_{y,metal} = \sqrt{-\beta_0^2 \epsilon_{r,metal} - \gamma_z^2} \tag{12}$$

And in a similar manner for the dielectric region we get

$$\alpha_{y,dielectric} = \sqrt{-\beta_0^2 \epsilon_{r,dielectric} - \gamma_z^2} \tag{13}$$

In (12) and (13)

β_0 is the free space wave number and ω is the angular velocity and are defined as

$$\beta_0 = \sqrt{\omega^2 \mu_0 \epsilon_0} = 2\pi/\lambda_0 \tag{14}$$

$$\omega = 2\pi f \tag{15}$$

Knowing that tangential electric fields are continuous across an interface, we can apply this boundary condition at y=0 we end up with the following relation:

$$\frac{\alpha_{y,dielectric}}{\epsilon_{r,dielectric}} = -\frac{\alpha_{y,metal}}{\epsilon_{r,metal}} \tag{16}$$

The last step is to solve for the complex propagation constant γ_z by using equations (12), (13) and (16). The propagation constant for the surface Plasmon-polariton mode of the waveguide depicted in A1 is:

$$\gamma_z = i\beta_0 \sqrt{\frac{\epsilon_{r,m}\epsilon_{r,D}}{\epsilon_{r,m} + \epsilon_{r,D}}} \tag{17}$$

APPENDIX B

Cutback Measurements of LRSPP waveguides cladded in Silica

The following measurements were performed in order to familiarize myself with the laboratory equipment and to gain valuable experience performing optical measurements.

Table B-1 shows insertion loss measurements of 8μm wide Au metal stripe waveguides cladded in Silica as discussed in[13]. Insertion loss measurements were carried out on five straight waveguides of various lengths. The LRSPP mode was excited through end-fire excitation using a polarization maintaining fibre at a free space wavelength of λ_0=1550nm. The expected theoretical attenuation was 2dB/mm and the expected total coupling loss was 1dB. From Figure B-1 the measured attenuation was 2.2dB/mm and the total coupling loss was 7.5dB. The error in the attenuation was -10% and the error in the coupling loss per facet was -650%. The R^2 fit of the measurements was 0.93 indicating that the measurements were indeed accurate. The high coupling loss is attributed to the end facets of the devices under test being dirt from residue left over from various matching fluids used during measurements.

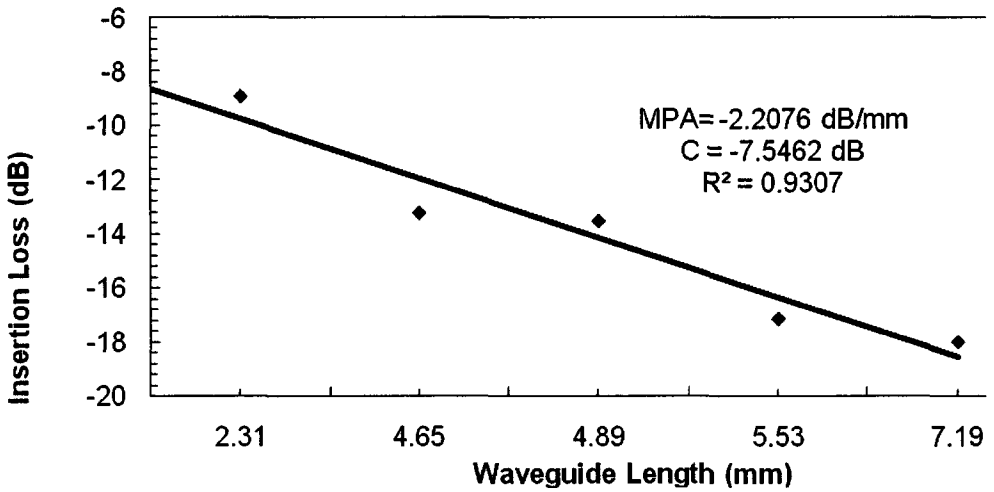

Figure B-1: Insertion loss measurements of five different straight Au stripe waveguides of different lengths cladded in silica.

APPENDIX C

The following index of refraction and thickness measurements were taken during the course of the research and are included for informational purposes. This table is also provided for some justification of the conclusions made regarding the index of refraction and thickness measurements.

Wafer ID	Measurement Type	λ_0 of Measurement	Index of Refraction	SD%	Thickness (μm)	SD%
Cytop_105	TE	632.8nm	1.3399	0.0200	1.5294	0.8000
Cytop_105	TM	632.8nm	1.3443	0.2900	1.4215	11.8600
Cytop_112	TE	1548nm	1.3347	0.0000	6.7066	0.3100
Cytop_130	TE	632.8nm	1.3402	0.0200	0.9975	0.4900
Cytop_133	TE	632.8nm	1.3398	0.0000	0.9142	0.3100
Cytop_136	TE	632.8nm	1.3441	0.0500	0.7631	0.6900
Cytop_137	TM	632.8nm	1.3458	0.1100	0.6376	1.8300
Cytop_147	TE	632.8nm	1.3399	0.0000	7.9010	0.4800
Cytop_147	TM	632.8nm	1.3399	0.0000	7.7240	3.0700
Cytop_147	TE	1312nm	1.3359	0.0000	7.7954	0.1800
Cytop_147	TM	1312nm	1.3355	0.0100	7.8703	2.6700
CT_REF	TE	632.8nm	1.3398	0.0000	8.2769	0.2200
CT_REF	TM	632.8nm	1.3398	0.0000	8.1463	1.6900
CT_REF	TE	1548nm	1.3340	0.0000	8.2726	0.5100
CT_REF	TM	1548nm	1.3351	0.1200	7.3633	17.1900
CT_4	TE	632.8nm	1.3412	0.0100	8.4711	0.1500
CT_4	TM	632.8nm	1.3389	0.1300	7.8720	2.2300
CT_4	TE	1312nm	1.3376	0.0000	8.4019	0.4500
CT_4	TM	1312nm	1.3372	0.0000	8.5499	1.6000